AGU PUBLICATIONS

JGR

Journal of Geophysical Research: Biogeosciences

RESEARCH ARTICLE
10.1002/2017JG004017

Key Points:
- The nutrient dynamics is controlled by the remineralization of organic matters induced by tidal fluctuation
- Significant N loss in the intertidal aquifer through nitrification or anammox attenuates the groundwater-borne nutrients input to the sea
- The DIP inputs to Tolo Harbour via SGD are mainly originated from the REM of organic matters

Supporting Information:
- Supporting Information S1

Correspondence to:
J. J. Jiao,
jjiao@hku.hk

Citation:
Liu, Y., Jiao, J. J., Liang, W., & Luo, X. (2017). Tidal pumping-induced nutrients dynamics and biogeochemical implications in an intertidal aquifer. *Journal of Geophysical Research: Biogeosciences*, *122*, 3322–3342. https://doi.org/10.1002/2017JG004017

Received 27 JUN 2017
Accepted 14 NOV 2017
Accepted article online 21 NOV 2017
Published online 27 DEC 2017

Tidal Pumping-Induced Nutrients Dynamics and Biogeochemical Implications in an Intertidal Aquifer

Yi Liu[1,2], Jiu Jimmy Jiao[1,2], Wenzhao Liang[1], and Xin Luo[1,2]

[1]Department of Earth Sciences, University of Hong Kong, Hong Kong, [2]Shenzhen Research Institute, The University of Hong Kong, Shenzhen, China

Abstract Tidal pumping is a major driving force affecting water exchange between land and sea, biogeochemical reactions in the intertidal aquifer, and nutrient loading to the sea. At a sandy beach of Tolo Harbour, Hong Kong, the nutrient (NH_4^+, NO_2^-, NO_3^-, and PO_4^{3-}) dynamic in coastal groundwater mixing zone (CGMZ) is found to be fluctuated with tidal oscillation. Nutrient dynamic is mainly controlled by tidal pumping-induced organic matter that serves as a reagent of remineralization in the aquifer. NH_4^+, NO_2^-, and PO_4^{3-} are positively correlated with salinity. Both NH_4^+ and PO_4^{3-} have negative correlations with oxidation/reduction potential. NH_4^+ is the major dissolved inorganic nitrogen species in CGMZ. The adsorption of PO_4^{3-} onto iron oxides occurs at the deep transition zone with a salinity of 5–10 practical salinity unit (psu), and intensive N-loss occurs in near-surface area with a salinity of 10–25 psu. The biogeochemical reactions, producing PO_4^{3-} and consuming NH_4^+, are synergistic effect of remineralization-nitrification-denitrification. In CGMZ, the annual NH_4^+ loss is estimated to be ~ 4.32×10^5 mol, while the minimum annual PO_4^{3-} production is estimated to be ~ 2.55×10^4 mol. Applying these rates to the entire Tolo Harbour, the annual NH_4^+ input to the harbor through the remineralization of organic matters is estimated to be ~ 1.02×10^7 mol. The annual NH_4^+ loss via nitrification is 1.32×10^7 mol, and the annual PO_4^{3-} production is ~ 7.76×10^5 mol.

1. Introduction

The hydrological cycle between land and ocean is crucial for the material exchange between terrestrial and oceanic environments. As a major component of land-sea hydrological cycle, submarine groundwater discharge (SGD) plays an important role in transporting of terrestrial materials (e.g., nutrients, carbon, and metals) to the sea (Moore, 2010). Therefore, SGD has received great attention from hydrologists, oceanographers, and geochemists globally since 1980s (Burnett et al., 2006; Cable et al., 1996; Johannes, 1980; Michael et al., 2005; Moore, 1996).

Nutrient elements such as nitrogen (N) and phosphate (P) are frequently investigated due to their impacts on the autotrophic production of organic matter (OM) in seawater (Joye & Anderson, 2008). Because the nutrient level is several orders of magnitude greater in groundwater than in seawater, SGD inputs a large amount of groundwater-borne nutrients to the sea and subsequently affects marine ecology (Johannes, 1980; Slomp & Van Cappellen, 2004). Meanwhile, nutrients derived by SGD are found to be comparable to riverine nutrient inputs in many studies (Burnett et al., 2007; Hwang, Kim, et al., 2005; Kroeger et al., 2007; Niencheski et al., 2007; Smith & Swarzenski, 2012; Sugimoto et al., 2015). SGD-derived nutrient loading is even the major external source for marine nutrient pool in some places such as Bangdu Bay, Korea (Hwang, Lee, et al., 2005), Masan Bay, Korea (Lee et al., 2009), Southern Yellow Sea, China (J. A. Liu et al., 2017), Mediterranean Bay, Palma Beach and Balearic Islands (Rodellas et al., 2014), Arctic Ocean and Gulf of Alaska (Lecher et al., 2016), Lynco Cove, Hood Canal, WA (Swarzenski et al., 2007), and Tampa Bay, Florida (Smith & Swarzenski, 2012). Groundwater-borne nutrients support the primary production and have impact on community structures of the phytoplankton in seawater (Lapointe, 1997; Luo et al., 2014). In addition, Paytan et al. (2006) found that nutrients, particularly nitrogen, necessary for the growth of coral reefs were derived from SGD. However, excessive land-sourced nutrient delivered by SGD motivates environmental or ecological problems. For instance, Laroche et al. (1997) suggested that nutrients induced by the increase of fertilizer use in 1970s were transported to the sea through SGD and resulted in the brown tide blooms in 1980s. Lee et al. (2010) pointed out that the outbreak of dinoflagellate red tide at southern sea of Korea was caused by a large

amount of inorganic nutrients inputs through SGD instead of Yangtze River discharge and oligotrophic Kuroshio warm current as suggested by previous studies (Choi, 2001; Yang et al., 2000).

As presented above, it is undeniable the noteworthy role of groundwater-borne nutrients played in marine environments and ecology. Currently, many SGD-delivered nutrient flux was estimated indirectly by multiplying the SGD flux with nutrient concentration in inland and nearshore groundwater end-members. However, two problems exist when applying this method. (1) Large uncertainties, which are derived from SGD estimation and the variation of nutrient concentration in groundwater end-members, make it difficult to accurately evaluate the influences of SGD-derived nutrients on marine environments. (2) This method neglects the chemical, biological, and geochemical transformation of nutrients during the transport in coastal aquifer. The coastal aquifer may act as a source of marine nutrient pool or a barrier preventing terrestrial nutrients discharging to the sea. Therefore, a better understanding of the spatial distribution and biogeochemical transformation of nutrients in coastal aquifer is essential for appropriately selecting groundwater end-members and quantifying global nutrient fluxes through SGD (Couturier et al., 2016; Moore, 2010).

Recently, besides SGD, many investigations focus on the transformation processes of nutrients in coastal aquifer. The mineral precipitation/dissolution and adsorption/desorption on metal oxides are main processes of phosphorus (P) in coastal aquifers (Santos et al., 2009; Spiteri et al., 2007). Since phosphorus is strongly absorbable to iron oxides (Beck et al., 2010; Slomp & Van Cappellen, 2004; Spiteri et al., 2008), the precipitation curtain of iron oxides in coastal groundwater mixing zone (CGMZ) may act as a sink for terrestrial phosphorus transporting to the sea (Charette & Sholkovitz, 2002; Rouxel et al., 2008). Nitrogen transformations in coastal aquifers contain many processes such as nitrification (NTR), denitrification (DNTR), nitrogen fixation (NFIX), dissimilatory nitrate reduction to ammonium (DNRA), remineralization (REM), and anammox (ANAM) (Joye & Anderson, 2008; Santoro, 2010). The investigations on cycling or the fate of N in intertidal sediments lead to many insightful findings (Couturier et al., 2016; Kroeger & Charette, 2008; Loveless & Oldham, 2010; Schlesinger, 2009; Schutte et al., 2015; Spiteri et al., 2008; Talbot et al., 2003). For example, Talbot et al. (2003) indicated that NH_4^+ moved conservatively while the loss of terrestrial NO_3^- was observed in CGMZ of Waquoit Bay, Massachusetts. However, the research of Kroeger and Charette (2008) at the same place indicated the concurrent removal of NH_4^+ and NO_3^- in freshwater and deep salinity transition zone. The possible removal mechanisms were heterotrophic or autotrophic DNTR, coupled NTR and DNTR, ANAM, and oxidation of NH_4^+ by Mn oxides. Through modeling reactive transport of nutrients in CGMZ, Spiteri et al. (2008) stated that the removal of terrestrial NO_3^- through DNTR was limited by the supply of dissolved organic carbon. They also suggested SGD as a significant source of NO_3^-. However, Couturier et al. (2016) found that NO_3^- delivered by terrestrial freshwater was transformed in shallow intertidal aquifer. The nitrogen discharged to ocean in a form of NH_4^+. The inconsistent findings indicate that variabilities of nitrogen processes in coastal sediments of different places were great due to the unique microbial communities, redox conditions, aquifer mineralogy, and hydrological controls. Schutte et al. (2015) found that nitrogen cycling in coastal sediments mitigated environmental effects of land-sourced nitrogen. However, as a byproduct of the nitrogen removal processes such AMAM, DNTR, and nitrifier DNTR, nitrous oxide (N_2O) is a potent greenhouse gas. Marchant et al. (2016) also confirmed the substantial N_2O production in permeable sediments of coastal aquifer. DNTR is usually regarded as a major sink of inorganic nitrogen in marine sediments and prevailing in suboxic and anoxic environments (Hulth et al., 2005). However, DNTR is found to have occurred in oxic environments (named aerobic DNTR) through N isotope paring techniques and laboratory experiments (Gao et al., 2009; Rao et al., 2007, 2008). The aerobic DNTR contributed to substantial N loss at continental shelf (Rao et al., 2007, 2008). The same N removal mechanism was also observed in intertidal aquifer (Gao et al., 2012). Except for aerobic DNTR, N loss can also be caused by coupled NTR-DNTR in permeable sediment of coastal aquifers (Marchant et al., 2014, 2016).

The transformation processes of phosphorus (P) and nitrogen (N) in coastal aquifers are influenced by many factors such as redox condition, aquifer heterogeneity, microbial communities, nutrient types in terrestrial groundwater, and hydrogeological variations. Kroeger and Charette (2008) pointed out that the N loss is not obvious in shallow salinity transition zone due to short groundwater residence time. Gonneea and Charette (2014) indicated that SGD-derived nutrient flux was doubled in summer compared to winter due to longer residence time in winter that strengthened N loss processes such as DNTR and ANAM in sediments. Through column experiments, Santos et al. (2012) revealed that flow velocity has potential effects on DNTR in

coastal sediments. Magalhães et al. (2005) suggested that NTR and DNTR were influenced by the availability of inorganic nitrogen. Teixeira et al. (2016) found that the activity of ANAM had a positive correlation with the increase of NO_2^-, but it was inhibited by the increase of NH_4^+. This is similar to NTR. Besides inorganic nitrogen availability, redox condition also influences the rates of ANAM (Teixeira et al., 2013; Teixeira et al., 2014), NFIX, and DNTR (Lee & Joye, 2006). Furthermore, redox conditions variation alters microbial communities for all functional groups that are crucial for nearly all transformation processes of nutrients in coastal aquifers (Santoro, 2010; Santoro et al., 2006, 2008).

Located at the northeast of New Territories, Hong Kong, Tolo Harbour is a semiclosed embayment with a surface area of 50 km^2 and a shoreline of 82 km (Luo & Jiao, 2016). Due to the bottlenecked coastline configuration and prevailing northeasterly wind direction, the water exchange with Mirs Bay, South China Sea is inefficient, which may result in a low removal efficiency of nutrients in harbor seawater (Lee et al., 2012). High frequency of algae bloom has been reported since 1980s (Xu et al., 2004). The Tolo Harbour Action Plan conducted in 1987 reduced 83% of biochemical oxygen demand and 82% of anthropogenic total nitrogen loading until 2008 (Lee et al., 2012). However, phytoplankton density increased from 4,000 to 25,000 cell mL^{-1} (Lie et al., 2011). The reduction of point loading nutrient sources did reduce the occurrence of red tide at Tolo Harbour area. The annual occurrence of red tide reduced from 13.3 in 1980s to 7.7 in 1990s and 5.4 in 2000s as reported by Agriculture, Fisheries and Conservation Department of Hong Kong. Even so, red tide occurrence is still very high recently (7.7 times per year since 2011), which demonstrates that nutrient loading by anthropogenic activity is not the only reason for red tide or algae blooms. Previous studies have demonstrated that nutrient (dissolved inorganic nitrogen, DIN; dissolved inorganic phosphorus, DIP; and SiO_2) loading by SGD was greater than by river discharge (Lee et al., 2012). This makes SGD-derived nutrients the major source of nutrients supporting the growth of algae and phytoplankton in the harbor (Lee et al., 2012; Luo et al., 2014; Luo & Jiao, 2016; Tse & Jiao, 2008). Through multiple geotracer-based models, Luo and Jiao (2016) found that groundwater-borne nutrients were 1–2 orders of magnitude greater than other nutrient sources. Their results also indicated the possible positive correlation between interannual SGD-derived nutrient loading and red tide outbreak.

As one of major driving forces of land-sea water exchange (Abarca et al., 2013; Heiss & Michael, 2014; Robinson et al., 2007), tidal pumping brings external nutrients to the coastal aquifer. Groundwater redox indicators such as salinity, pH, dissolved oxygen (DO), oxidation/reduction potential (ORP), and temperature are also found to be oscillated with tidal fluctuation (Liu, Jiao, & Liang, 2017). Under such circumstances, to investigate tidal fluctuation-influenced nutrient dynamics and its potential biogeochemical transformations in CGMZ, a series of sampling campaigns along a transection perpendicular to the shoreline at different tidal stages were conducted in this study. In this way, a better understanding of the influencing mechanism of tidal fluctuation on the nutrient dynamics is expected to be obtained.

2. Material and Methods

2.1. Study Site

The sampling site (22°28′ 06.91″N, 114°13′02.22″E) is located at a sandy beach of Ting Kok, Tolo Harbour, Hong Kong. From land to sea, surficial sediments mainly contain Quaternary deposits such as river and beach sediments originated from decomposed volcanic rock (woodland area in Figure 1). The shore (mangrove zone and sandy beach in Figure 1) sediments are mainly enriched in littoral pebbles, tidal sand dunes, tidal muds, fluvial pebbles or cobbles, sea shells, and some gravels. In the abandoned paddy field, sediments are much finer and are enriched in loam, clay, and finer sand (Chan et al., 1995). Falling head (Li et al., 2010) and constant head (Amoozegar, 1989) permeability tests were carried out to measure hydraulic conductivity of the sediments. The estimated hydraulic conductivity is ~ 0.42 m/d in paddy field, ~ 1.6 m/d in mangrove zone, and ~ 4.49 m/d at sandy beach. The porosity of sediments was measured to be ~ 0.3 in laboratory following the standard procedure (Fetter, 2000). The slope of sandy beach is ~ 1:100. The annual mean sea level is ~1.45 mPD (meter above principal datum) with an average tidal range of ~ 1.06 m. The typical hydraulic gradient is about 0.04 and the typical advection velocity is 0.2 m/d according to Darcy's Law (Liu, Jiao, & Liang, 2017). With the fluctuation of tidal level, the flow velocity oscillates around the typical advection velocity accordingly. The measured tidal level during the sampling period is illustrated in Figure 2. The sea level ranges from ~ −1.02 mPD to ~ 0.8 mPD with the highest tidal level observed during 7:00 a.m. to

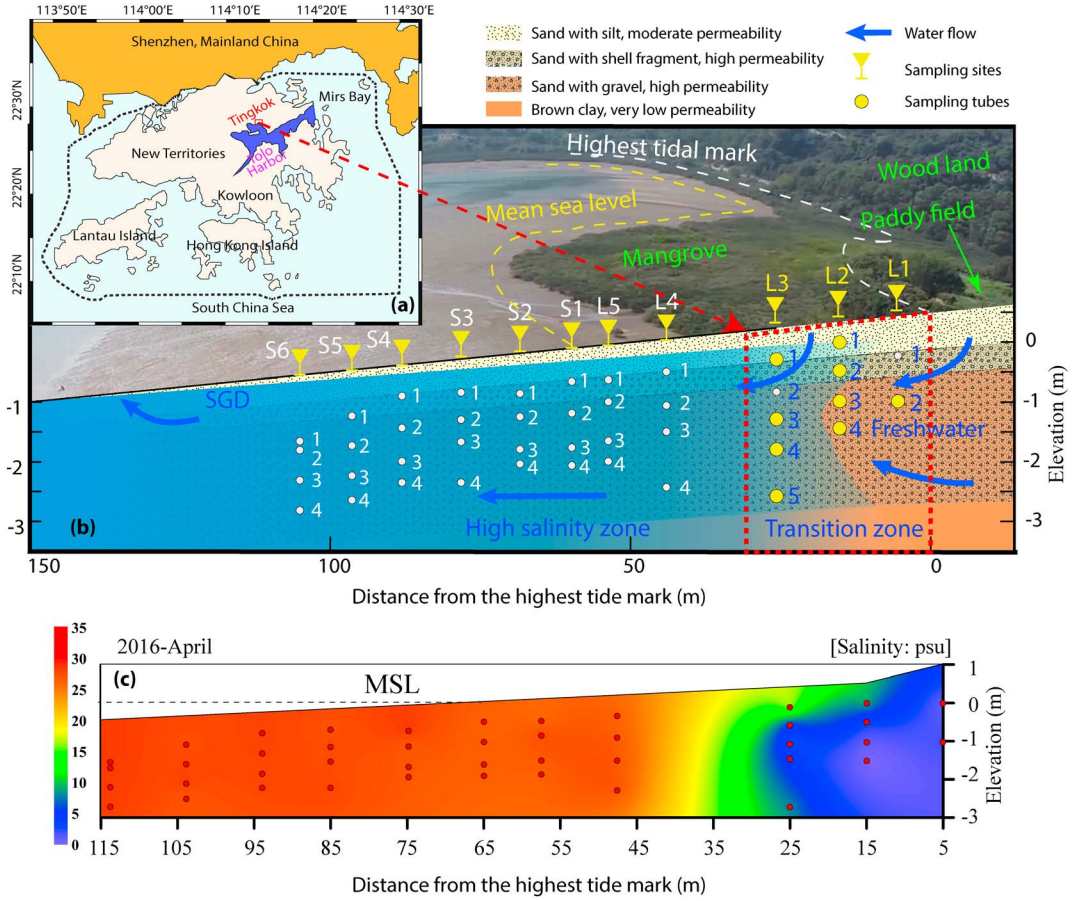

Figure 1. (a)The location of the study site, (b) the multilevel permanent sampling system installed in the field, and (c) the salinity of groundwater along the sampling transection on 25 April 2016. Sampling points are indicated by circles in Figure 1a, and for the study discussed in this paper, only the points indicated by yellow dots are sampled.

12:00 a.m. and the lowest tidal level observed during 17:00 p.m. to 18:00 p.m. The infiltration depth is ~ 1 m according to the total alkalinity data (Liu, Jiao, Liang, et al., 2017).

A permanent multilevel sampling system (Luo et al., 2017) was installed in a transection perpendicular to the shoreline at Ting Kok (Liu, Jiao, Liang, et al., 2017). The system contains 11 sampling sites (namely L1 to L5, and S1 to S6) at different locations along a shore-perpendicular sampling transection, and each sampling site

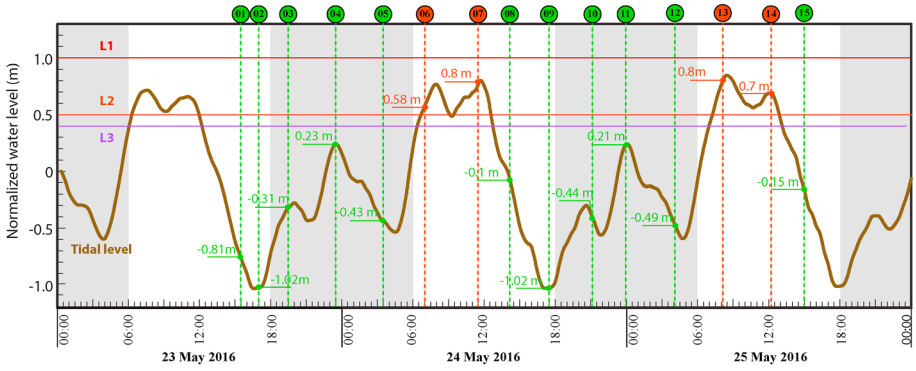

Figure 2. The tidal fluctuation during the sampling period. The horizontal lines denote the ground surface of the sampling sites at L1 (red), L2 (orange), and L3 (purple). The tidal level at each sampling round (SR) is denoted at the intersection of vertical dash line. The SR number is denoted at the top, and red color means the tidal level surpassed the ground elevation of L2 and L3. The gray background and white background represent the night and daytime, respectively.

has 2–5 sampling tubes with different depths (Figure 1). The 43 sampling tubes in this system constitute a 2-D sampling transection (about 110 m long and 3 m deep). In the study on nutrient dynamic, only three sites (L1, L2, and L3, or filled circles in Figure 1) are sampled because they are located in the salinity transition zone according to the spatial distribution of salinity (Figure 1). L1 has two sampling tubes (L1-1 and L1-2) and only one (L1-2 with a depth of 2 m) was sampled. All four sampling tubes in L2 (L2-1 to L2-4, with depths of 0.5, 1, 1.5, and 2 m) were sampled in this study. Four of five sampling tubes (L3-1, L3-3 to L3-5, with the depths of 0.5, 1.5, 2, and 3 m) in L3 were sampled because L3-2 (depth of 1 m) was clogged. As for the salinity and stable isotopes, groundwater from all sampling tubes was collected.

2.2. Sample Collection

Fifteen rounds of groundwater sampling (called sampling round (SR) hereafter) were conducted during 48 h from 23 to 25 May 2016 with time interval about 3 to 4 h (Figure 2). According to tidal levels at different SRs and the elevations of sampling sites plotted in Figure 2, seawater submerges L2 and L3 at SRs 06, 07, 13, and 14. At SRs 02 and 09, the tidal level is the lowest (1.02 m below the mean sea level) during the sampling period. L1 is not submerged by seawater throughout the sampling period. At each SR, nine groundwater samples (with a volume of 0.5–1 L for each sample) from three sampling sites (Figure 1) were pumped at the same time with peristatic pumps preinstalled at each site and preconnected to each sampling tube. Meanwhile, one nearshore seawater sample (with a volume of 4 L) was collected. During the sampling period, 150 samples in total were collected for nutrient (NH_4^+, NO_2^-, NO_3^-, and PO_4^{3-}) analyses. Samples for stable isotope (δ^2H and $\delta^{18}O$) analyses were collected on 25 April 2016. Groundwater pumped at the beginning of each sampling was discarded to avoid the influence of residual water in tubes since previous sampling. Groundwater was filtered in situ with the 0.45 μm syringe filter before placed in acid-washed centrifuge tubes (50 mL). Nutrient samples were first stored in an ice box in the field and then transported back to laboratory storing in frozen environment (−18°C). Groundwater samples for stable isotopes (δ^2H and $\delta^{18}O$) analysis fully fill in small centrifuge tubes (1.5 mL) after the filtering process. The sample tubes were sealed with parafilm and stored in refrigeration environment (4°C) to prevent evaporation.

2.3. Analytical Methods

Indicators of redox condition such as salinity, pH, DO, and ORP were measured immediately after sample collection with a portable multiparameter meter (Hanna HI 98194). Resolutions and accuracies of redox indicators are 0.01 and ±0.01 psu for salinity, 0.01 and ±0.02 pH for pH, 0.01 and ±0.10 ppm for DO, and 0.1 and ±1.0 mV for ORP. The pH and platinum pin ORP sensor, four-ring stainless steel conductivity sensor, and galvanic DO sensor of the meter were precalibrated with a standard solution (Hanna Instruments) in the laboratory. Concentrations of nutrients (NH_4^+, NO_2^-, NO_3^-, and PO_4^{3-}) were measured on a Lachat Instruments Quickchem 8000 flow injection analyzer using standard colorimetric techniques within 1 week of sampling. Analytical errors are $<10\%$ for NH_4^+, $<8\%$ for NO_2^-, $<3\%$ for NO_3^-, and $<5\%$ for PO_4^{3-}. Stable isotopes (δ^2H and $\delta^{18}O$) were analyzed with Off-axis integrated cavity output spectroscopy (OA-ICOS) laser adsorption spectrometer. Water samples were introduced into OA-ICOS via a PAL HTC-*xt* autoinjector. δ^2H and $\delta^{18}O$ were measured simultaneously within 90 s at each injection. Each sample was injected 6 times, and the last four results were averaged as the final result. The precisions of measurements are $<0.5‰$ and $<0.1‰$ for δ^2H and $\delta^{18}O$, respectively.

3. Results

3.1. Stable Isotopes and Water Patterns

The stable isotope results represent the first measurements of δ^2H and $\delta^{18}O$ in groundwater of intertidal aquifer at Tolo Harbour. Spatial distributions of stable isotopes (δ^2H and $\delta^{18}O$) are shown in Figures 3a and 3b. δ^2H ranges from −38.3‰ to −10.3‰ while $\delta^{18}O$ ranges from −6.08‰ to −1.85‰ (Table S1). The near-surface area closed to the sea is enriched in heavy isotopes, and the inland deeper area is isotopically depleted in both δ^2H and $\delta^{18}O$. Stable isotopic compositions of fresh groundwater (FGW) from L1-1 (−28.32‰ and −4.99‰ for δ^2H and $\delta^{18}O$) and L1-2 (−23.43‰ and −4.58‰ for δ^2H and $\delta^{18}O$) are different from the compositions of FGW from L2-3 (−35.31‰ and −5.69‰ for δ^2H and $\delta^{18}O$) and L2-4 (−38.03‰ and −6.08‰ for δ^2H and $\delta^{18}O$). The dramatic variation of δ^2H and $\delta^{18}O$ within such a short distance (10 m) indicates the different origins of FGW from L1 (L1-1 and L1-2) and L2 (L2-3 and L2-4). Plot of δ^2H versus $\delta^{18}O$ (Figure 3c)

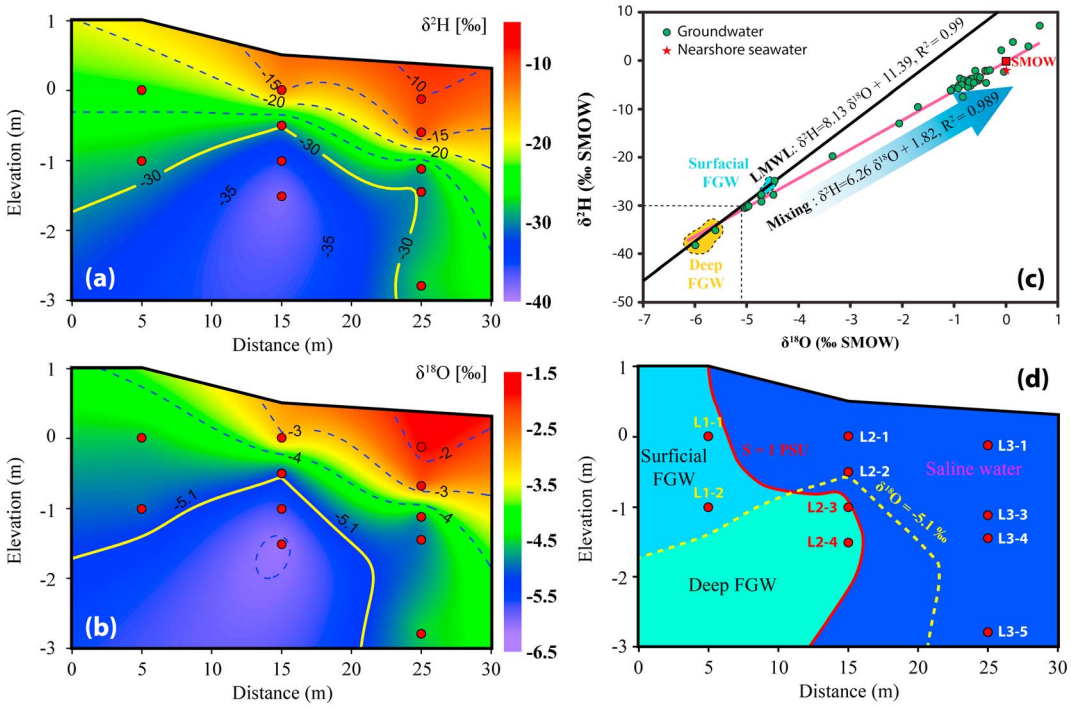

Figure 3. Spatial distributions of (a) δ^2H and (b) $\delta^{18}O$ in the sampling site, (c) scatterplot of δ^2H versus $\delta^{18}O$, and (d) groundwater patterns separated by salinity and stable isotopic compositions. The LMWL and SMOW in Figure 3c are local meteoric water line and standard mean ocean water, respectively.

also clearly presents the differences in isotopic composition in these two groups of FGW. The δ^2H and $\delta^{18}O$ in FGW from both groups of FGW are in the local meteoric water line (LMWL) in Hong Kong, which can be presented by the equation $\delta^2H = 8.13\ \delta^{18}O + 11.39$ (Li et al., 2012). The LMWL is highly identical to the global meteoric water line described as $\delta^2H = 8.0\ \delta^{18}O + 10$ (Craig, 1961). Therefore, this study merely uses LMWL as a reference. Groundwater sample scatters of δ^2H and $\delta^{18}O$ (Figure 3c) are in a line between FGW and nearshore seawater (standard mean ocean water, SMOW), suggesting that mixing process dominates the stable isotopic composition of groundwater in the study area. The mixing line can be described by the equation $\delta^2H = 6.26\ \delta^{18}O + 1.82$ with a high R^2 value of 0.989. According to salinity and stable isotopic composition, the groundwater in this sampling transection is separated into three water patterns, that is, surficial FGW (L1-2), deep FGW (L2-3 and L2-4), and saline water (L2-1, L2-2, and L3-1 to L3-5) (Figure 3d). FGW and saline water are separated by salinity (S = 1 psu), while surficial FGW and deep FGW are separated by an averaged value of stable isotopes (either $\delta^2H = -30‰$ or $\delta^{18}O = -5.1‰$) from sites L1 and L2. Either line of $\delta^2H = -30‰$ or $\delta^{18}O = -5.1‰$ can be used for the separation because both lines are analogous between 0 and 15 m.

3.2. Ammonium (NH_4^+) Dynamic

The NH_4^+ dynamic is illustrated in Figure 4. Generally, NH_4^+ concentration in surficial FGW (12.27 μM) is much higher than that in deep FGW (0.84 μM) and saline water (2.94 μM) (Table 1). NH_4^+ in saline water only exists in near-surface area where nearshore seawater enters the aquifer suggesting that NH_4^+ is originated from nearshore seawater. From SRs 01 to 05, tidal levels are lower than the beach surface (Figure 2); thus, the depleted NH_4^+ in saline water is mainly led by biogeochemical reaction instead of seawater dilution. However, at SR 04 the depletion of NH_4^+ is hindered probably owing to a lower intensity of biogeochemical activities (middle night). In addition, DNTR increases with flow velocity when the advection velocity is smaller than 0.72 m/d as indicated by Santos et al. (2012). The typical advection velocity of this study is ~ 0.2 m/d (Liu, Jiao, & Liang, 2017), which is within the range in which the DNTR increases with the velocity. Therefore, the comparative high tidal level at SR 04 (0.23 m) lowers the flow velocity and subsequently hinders the removal efficiency of NH_4^+ by biogeochemical reactions. The seawater submerges the beach surface

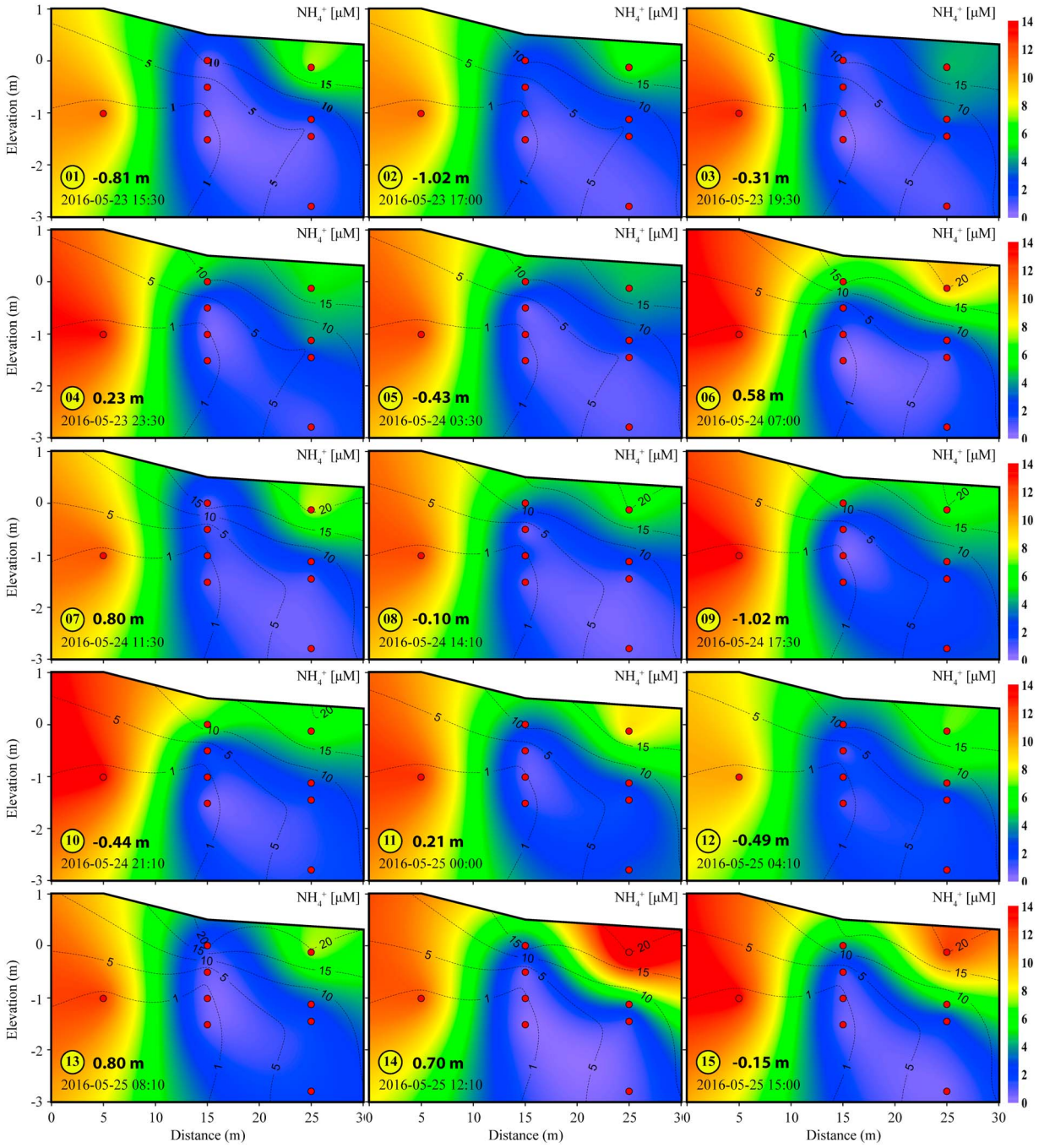

Figure 4. The dynamics of NH_4^+ at different tidal stages. The SRs and corresponding sampling time and tidal level are denoted at the left bottom corner. The black lines are contour lines of salinity.

of L2 and L3 at SRs 06 and 07. The NH_4^+ concentration in saline water increases accordingly and reaches a comparatively high concentration (Figure 4). For example, from SRs 05 to 06, the NH_4^+ concentrations at L3-1 and L2-1 increase from 4.45 to 9.56 μM and 4.03 to 5.39 μM, respectively (Table S2). Since NH_4^+ concentration in nearshore seawater (1.93 μM) is low, the high concentration of NH_4^+ in saline water is definitely transformed from organic form of nitrogen (dissolved organic nitrogen or particulate organic nitrogen). Therefore, NH_4^+ stems from REM of organic matters induced by seawater infiltration at high tide. Additionally, identical trends of rising salinity (black line with numbers in Figure 4) and NH_4^+ (color contour in Figure 4) indicate that the infiltration of seawater at high tide is the causative factor of high

Table 1
The Average Value of Nutrients in Different Water Patterns During the Sampling Period

Water patterns	NH_4^+ (μM)	Std	NO_2^- (μM)	Std	NO_3^- (μM)	Std	PO_4^{3-} (μM)	Std	N:P
Surficial FGW[a]	12.27	1.05	0.09	0.06	0.34	0.31	0.26	0.05	49
Deep FGW[b]	0.84	0.54	0.12	0.07	0.56	0.5	0.10	0.03	18
Saline water[c]	2.94	2.82	0.29	0.36	0.23	0.29	1.25	2.03	20
Seawater	1.93	1.51	0.19	0.12	0.50	0.32	0.16	0.14	23

[a]The value is averaged from L2-3 and L2-4. [b]The value is averaged from L1-2. [c]The value is averaged from L2-1, L2-2, L3-1, L3-3, L3-4, and L3-5.

NH_4^+ in saline water. The second tidal cycle (SRs 08 to 15) shows a uniform trend as the first one (SRs 01 to 07). From SR 10 to SR 11, a slight increase of NH_4^+ in saline water at near-surface area has a similar reason with the increase of NH_4^+ from SR 03 to SR 04. The time interval between SR 04 and SR 11 is exactly one tidal cycle (24 h) that indicates NH_4^+ fluctuates with tidal oscillation.

3.3. Nitrite (NO_2^-) Dynamic

The NO_2^- presented in Figure 5 shows rather different spatial distributions and temporal variations compared to NH_4^+. Generally, NO_2^- concentration in surficial FGW (L1-2) is 0.09 μM, which is 2 orders of magnitude lower than NH_4^+ concentration (12.27 μM) (Table 1). With an average value of 0.12 μM, the NO_2^- is slightly higher in deep FGW (L2-3 and L2-4) than in surficial FGW. NO_2^- in saline water (0.29 μM) is the highest among the three water patterns (Table 1). In saline water, NO_2^- concentration varies with tidal oscillation. However, the spatial and temporal distributions of NO_2^- are distinguishing from NH_4^+. Two reasons may explain the dissimilarity. First, NO_2^- is not originated from nearshore seawater because of a low NO_2^- concentration in seawater (0.19 μM). Second, most of NO_2^- in saline water is transformed from NH_4^+ through NTR (oxic condition when DO >20 μM) or from NO_3^- through DNRA (suboxic or anoxic condition when DO <20 μM) because all external mixing end-members (surficial FGW, deep FGW, and nearshore seawater) are deleted in NO_2^-. The efficiency of microbial activities that results in the depletion and production of NO_2^- in saline water is influenced by various factors such as DO, temperature, and flow rates. Since time requirement for the transformation from NH_4^+ to NO_2^-, the variation of NO_2^- lags behind the change of NH_4^+. This can be demonstrated by the fact that high NH_4^+ concentration in saline water is observed at high tide (e.g., SR 06), while high NO_2^- concentration in saline water occurs 12 h later (SR 11). During the first tidal cycle (SRs 01 to 07), NO_2^- concentration in saline water increases initially and peaks at SR 04 and then drops afterward (Figure 5). For example, NO_2^- concentration at L3-1 climbs from 0.18 μM at SR 01 to 2.23 μM at SR 04 and then falls to 0.19 μM at SR 07 (Table S2 in the supporting information). During the second tidal cycle (SRs 08 to 15), similar spatial distribution and temporal variation of NO_2^- in saline water is observed and the NO_2^- concentration peaks at SR 11. Note that the time interval between SR 04 and SR 11 is exactly one tidal cycle. Thus, temporal variation of NO_2^- in saline water is directly regulated by tidal fluctuation. All relative high concentration of NO_2^- is observed at low tidal level (−0.31 m, 0.23 m, −0.43 m for SRs 03, 04, and 05 and −0.44 m, 0.21 m, and −0.49 m for SRs 10, 11, and 12). This is mainly because more air oxygen enters the aquifer and high DO water from fresh FGW flows seaward much more easily at low tide, which strengthens NO_2^- production from NH_4^+ through NTR in oxic condition (The DO at L2-1 is ~ 42.5 μM during SRs 03 to 05 and ~ 35.42 μM during SRs 10 to 12, while the DO at L3-1 is ~ 39.48 μM during SRs 03 to 05 and ~ 43.13 μM during SRs 10 to 12). The tidal level is increasing from SRs 03 to 04, but it is still lower than the groundwater level at L3 and L2. Groundwater flow direction remains unchanged from land to sea, but the flow velocity is reduced. The low advective velocity at SR 04 is also a major driver of a low removal efficiency of NO_2^- by DNTR, which in return contributes to NO_2^- accumulation in saline water.

3.4. Nitrate (NO_3^-) Dynamic

The spatial distribution and temporal variations of NO_3^- are shown in Figure 6. Generally, NO_3^- concentration in surficial FGW, in deep FGW, and in saline water is 0.34 μM, 0.56 μM, and 0.23 μM, respectively (Table 1). As discussed previously, high NH_4^+ concentration mainly exists in surficial FGW while high NO_2^- concentration mainly exists in saline water. However, high NO_3^- concentration is mainly observed in deep FGW. The comparatively high NO_3^- plumes in deep FGW are observed at relatively low tidal level (SRs 02, 03, 08, 09,

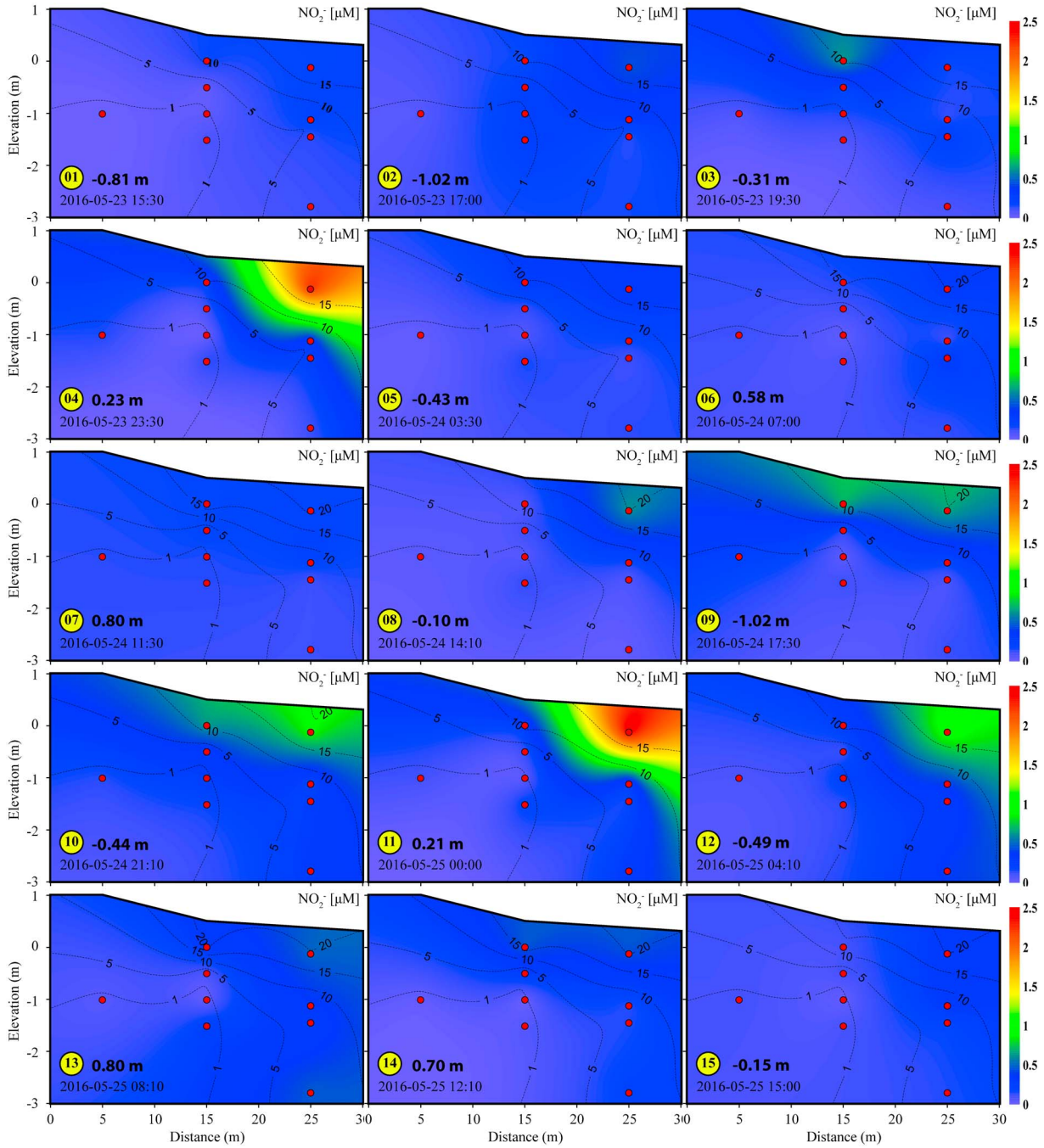

Figure 5. The dynamics of NO_2^- at different tidal stages. The SRs and corresponding sampling time and tidal level are denoted at the left bottom corner. The black lines are contour lines of salinity.

11, and 12). This is because low tidal level benefits the upwelling of deep FGW with high NO_3^- concentration. When SRs have similar tidal levels, they have a similar plume shape and also a similar variation trend even though some divergence occurs in concentrations of NO_3^-. This can be demonstrated by that the variation of NO_3^- plume from SRs 06 to 08 is very similar to that from SRs 13 to 15 while the variation from SR 04 to SR 05 is also similar to that from SR 11 to SR 12. The enrichment of NO_3^- from L3-1 at SRs 04 and 11 (Figure 6) has a similar reason as enrichment of NO_2^- due to the fact that the NO_3^- at this location is mainly transformed from NO_2^-. The low tidal level results in more oxygen entering the aquifer, which strengthens the transformation of NO_3^- from NO_2^- via NTR in oxic condition. The comparatively

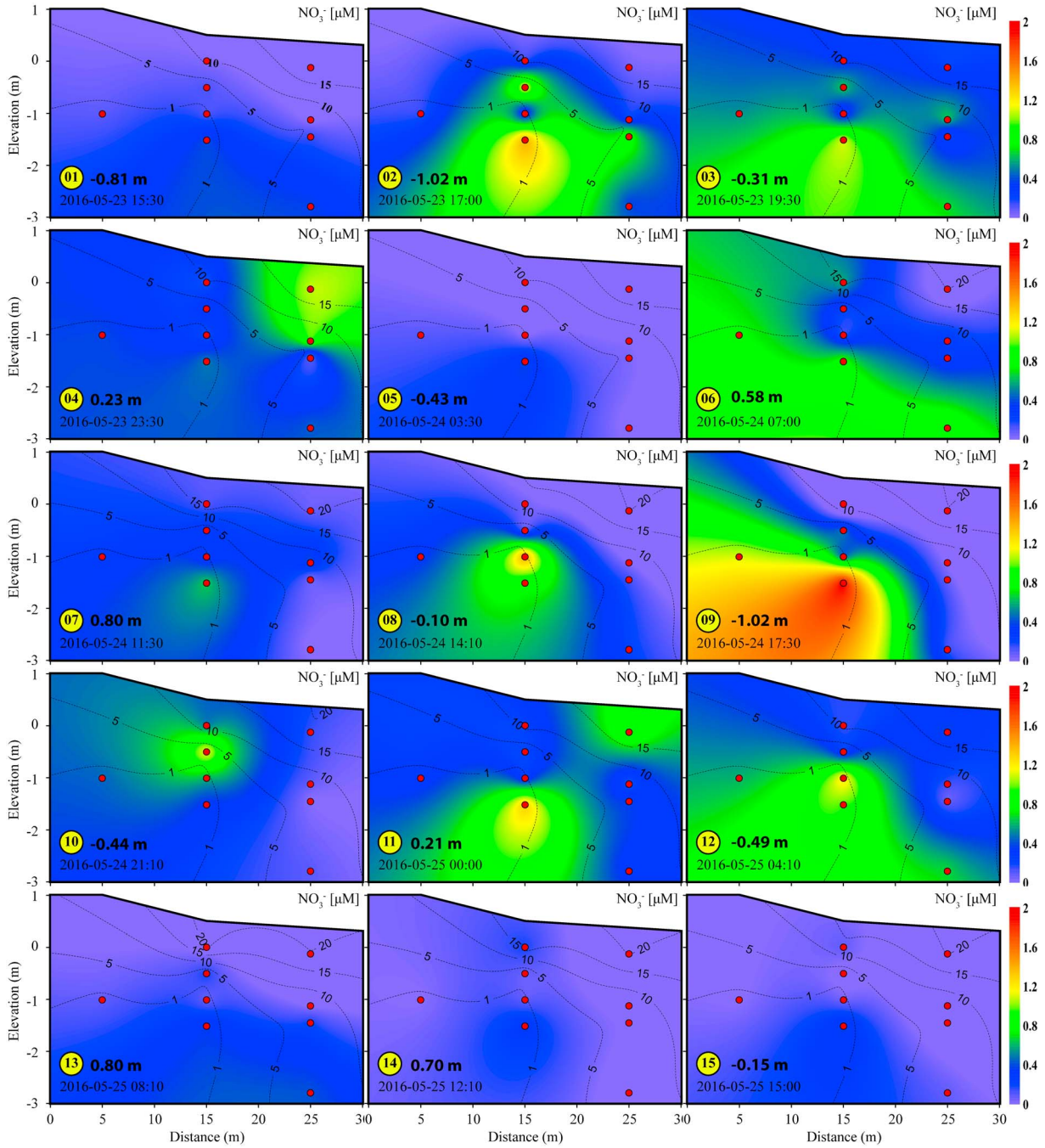

Figure 6. The dynamics of NO_3^- at different tidal stages. The SRs and corresponding sampling time and tidal level are denoted at the left bottom corner. The black lines are contour lines of salinity.

high concentrations of NO_2^- at SRs 04 and 11 (Figure 5) also strengthen NTR and hinder the DNRA or DNTR. These periodic variations indicate that NO_3^- dynamic is highly influenced by tidal fluctuation or tidal fluctuation-induced variation of microbial activities.

3.5. Phosphate (PO_4^{3-}) Dynamic

Figure 7 presents PO_4^{3-} dynamic. PO_4^{3-} concentrations in surficial FGW and deep FGW are 0.26 μM and 0.10 μM, respectively (Table 1). The average PO_4^{3-} concentration in saline water is 1.25 μM (Table 1). Note that high PO_4^{3-}concentrations are mainly observed in near-surface area (L2-1 and L3-1). For example, the

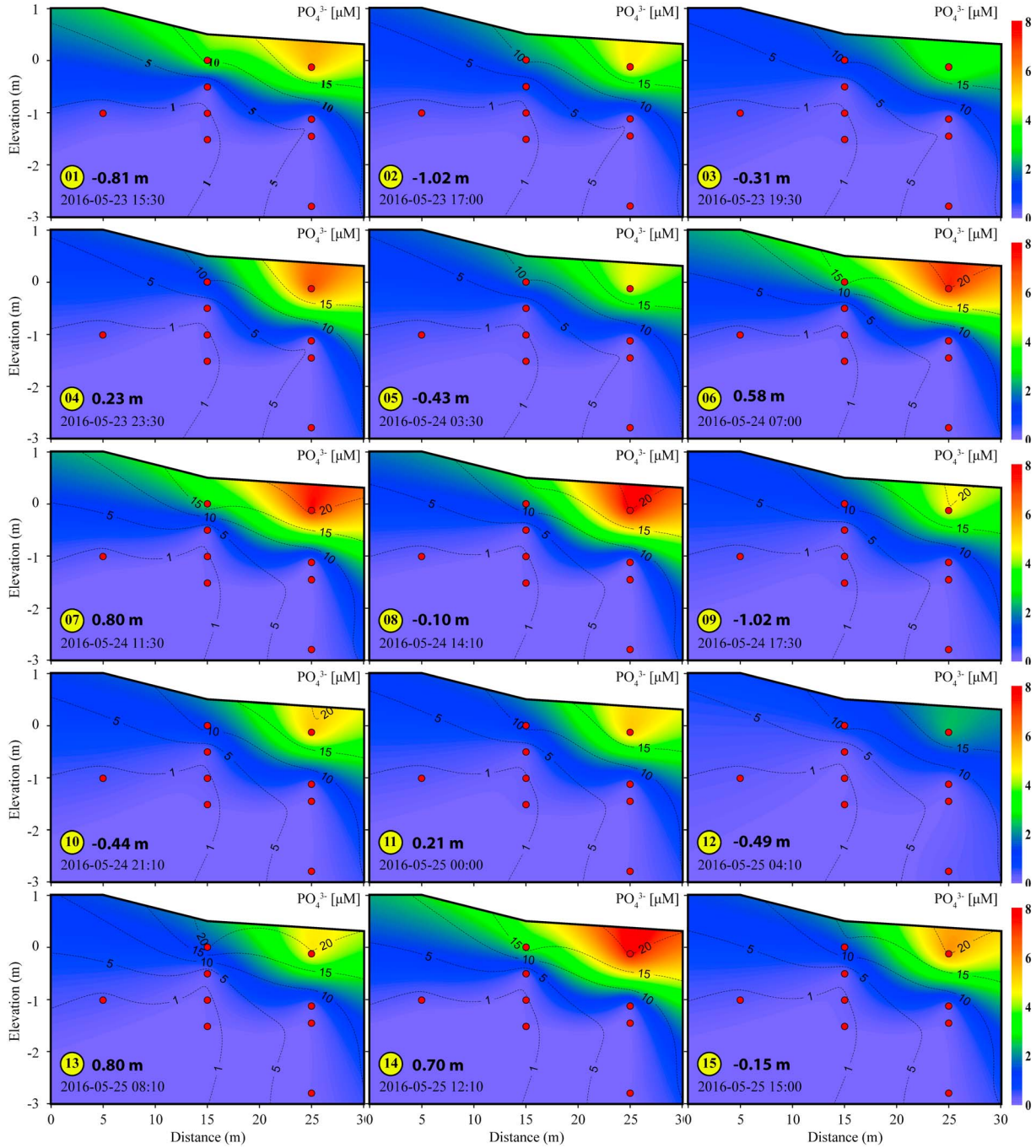

Figure 7. The dynamics of PO_4^{3-} at different tidal stages. The SRs and corresponding sampling time and tidal level are denoted at the left bottom corner. The black lines are contour lines of salinity.

average value of PO_4^{3-} is much higher at L3-1 than that in saline water (5.61 versus 1.24 μM in Table S2). Since PO_4^{3-} in nearshore seawater is very low (0.16 μM), the PO_4^{3-} in near-surface area is transformed from organic phosphorus induced by seawater infiltration. A comparison of NH_4^+ (Figure 4) and PO_4^{3-} dynamic (Figure 7) shows an identical variation in saline water especially in near-surface area. Specifically, both PO_4^{3-} and NH_4^+ concentrations in near-surface area decline from SRs 01 to 03, rebound at SR 04, and then drop again at SR 05. PO_4^{3-} and NH_4^+ in near-surface area climb to peak values when seawater submerges ground surface of L2 and L3 at SRs 06 and 07. A repeated variation is observed at second tidal cycle (SR 08 to SR 15). The identical PO_4^{3-} and NH_4^+ dynamic in near-surface area confirms the same

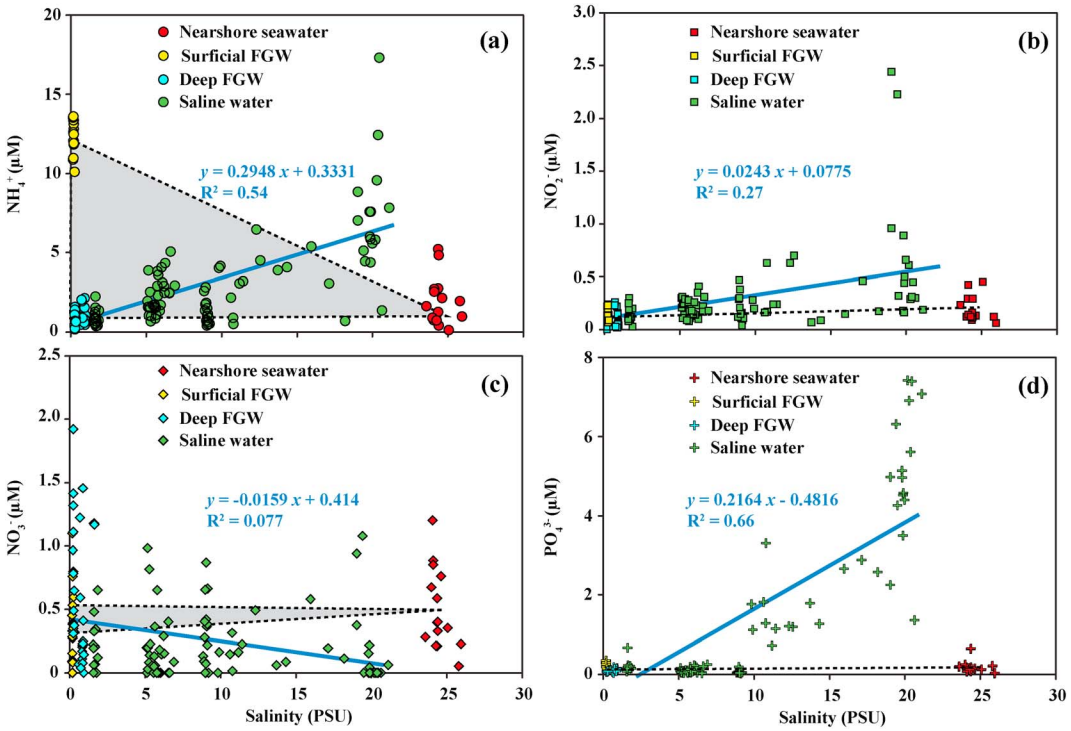

Figure 8. (a) NH_4^+ versus salinity, (b) NO_2^- versus salinity, (c) NO_3^- versus salinity, (d) PO_4^{3-} versus salinity. The gray polygon is drawn according to the conservative mixing between the three end-members (surficial FGW, deep FGW, and nearshore seawater). The three end-members' values are the average values of surficial FGW, deep FGW, and nearshore seawater, respectively, during the sampling period. In Figures 8b and 8d, the mixing line between surficial FGW and nearshore seawater and that between the deep FGW and nearshore seawater coincide with each other and become one line.

transformation pathway from REM of organic matters infiltrated with the seawater. Furthermore, the PO_4^{3-} plumes at different tidal stages are shaped by the low PO_4^{3-} concentrations at L3-3. The configuration of PO_4^{3-} is attributed to the high content of iron oxides in the deep location of transition zone. The iron oxides have strong adsorption ability to PO_4^{3-}, which leads to the low concentration of PO_4^{3-} in saline water at L3-3.

4. Discussion

4.1. Nutrient-Salinity Relationships

NH_4^+ concentration varies significantly in different water patterns as shown in Figure 4 and Table S2. The NH_4^+-salinity relationship (Figure 8a) shows that NH_4^+ scatters with high salinity are located outside the triangle zone (conservative mixing of surficial FGW, deep FGW, and nearshore seawater). This suggests the intensive biogeochemical reactions of NH_4^+ in aquifer. NH_4^+ in high salinity seawater is low (1.92 μM); however, NH_4^+ in saline water with higher proportion of seawater holds a higher concentration (positive correlation with salinity with $R^2 = 0.54$, $p < 0.0001$). This confirms that NH_4^+ in saline water is transformed from REM of organic matters carried by nearshore seawater but not directly from NH_4^+ in nearshore seawater. Additionally, although NH_4^+ concentration in surficial FGW is high (12.27 μM), NH_4^+ scatters with the salinity $< \sim 15$ psu falls far below the conservative mixing line between surficial FGW and nearshore seawater. This indicates the removal of NH_4^+ in surficial FGW by biogeochemical reactions (e.g., NTR) in coastal aquifer. Meanwhile, the majority of NO_2^- scatters fall above the theoretical conservative mixing line between FGW and nearshore seawater (Figure 8b) indicating the production of NO_2^-. NO_2^- in saline water increases with the salinity ($R^2 = 0.27$, $p < 0.0001$) (Figure 8b), which is very similar to the distribution of NH_4^+ in saline water. This confirms the transformation of NO_2^- from NH_4^+ through NTR. The decreasing trend of NO_3^- and comparatively low concentration of NO_3^- (most of NO_3^- smaller than 1 μM) shown in Figure 8c confirms that

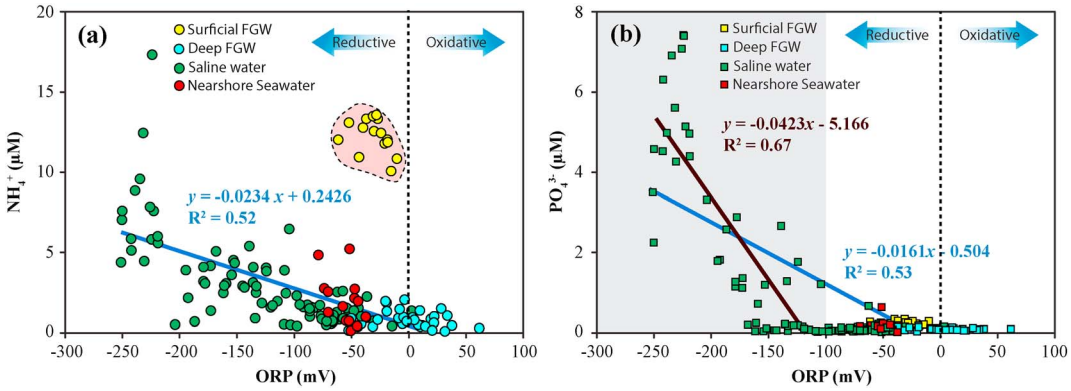

Figure 9. (a) NH_4^+ versus ORP, and (b) PO_4^{3-} versus ORP. The dark fitting line in Figure 9b is made by the data with ORP < -100 mV.

NO_2^- in saline water is unlikely produced via DNRA from NO_3^-. In addition, the large variation of NO_3^- at each sampling tube reflects the effect of tidal fluctuation on NO_3^-. PO_4^{3-} scatters shown in Figure 8d indicate that the majority of PO_4^{3-} is produced in the aquifer due to relatively low PO_4^{3-} concentrations in mixing end-members (0.26 μM for surficial FGW, 0.10 μM for deep FGW, and 1.25 μM for nearshore seawater). Similar to NH_4^+, PO_4^{3-} in saline water increases with salinity ($R^2 = 0.66$, $p < 0.0001$), which confirms that the production of PO_4^{3-} in saline water has the same pathways as NH_4^+. Moreover, a better linear fitting is observed with the salinity $>$ ~ 5 psu, which indicates that PO_4^{3-} production in the low salinity saline water is not obvious owing to the limited organic matters from nearshore seawater. The configuration of low PO_4^{3-} and high NH_4^+ in surficial FGW suggests that NH_4^+ is originated from external sources instead of local production via REM of organic matters.

4.2. Nutrient-ORP Relationships

As shown in Figure 9a, with the increase of ORP, NH_4^+ in pore water of the intertidal aquifer decreases. NH_4^+ scatters in surficial FGW are far away from those scatters in other water patterns because of their unique origins. In this study, NH_4^+ shows a declining trend along with the increase of ORP from −250 to 50 mV. This is different from the results of Santos et al. (2008). In their study, NH_4^+ concentration peaks in a slightly reductive area (−100 mV). The negative correlation between NH_4^+ and OPR indicates that NH_4^+ is more likely to exist in the reductive environments. This is because the electron receivers in oxidative environment facilitate NTR processes, which could significantly decreases NH_4^+ concentration. In oxidative environment, although NH_4^+ prefers to desorb from aquifer solid grains, the desorbed NH_4^+ does not compensates the consumption of NH_4^+ in water by improved NTR process (Morse & Morin, 2005). Under such circumstances, the adsorption is not the major removal process of NH_4^+, which highlights the importance of biogeochemical reactions such as NTR, DNRA, and ANAM in the accumulation or removal of NH_4^+ in the aquifers (Joye & Anderson, 2008). Likewise, PO_4^{3-} in pore water also reduces with the increase of ORP (Figure 9b). A similar trend was also found in the study of nutrient biogeochemistry in an intertidal aquifer at Gulf of Mexico (Santos et al., 2008). The decline rate of PO_4^{3-} concentration is larger when ORP is smaller than −100 mV (Figure 9b). The reason is analogous to the steeper increase rate of PO_4^{3-} with the salinity $>$ ~ 5 psu (Figure 8d). Very limited PO_4^{3-} is observed at slightly reductive (−100 mV $>$ ORP $>$ 0 mV) and oxidative environments (ORP $>$ 0 mV), which is different from the result of Santos et al. (2008). In their study, a very high concentration of PO_4^{3-} (10 μM) was found at oxidative environment (ORP $>$ 100 mV). This difference is mainly caused by the different controlling factors of the PO_4^{3-} distribution. In this study, the distribution of PO_4^{3-} is mainly controlled by PO_4^{3-} production via REM of organic matter induced by nearshore seawater, instead of the other influencing factors such as the adsorption onto negatively charged clays or the coprecipitation with other dissolved species (Paytan & McLaughlin, 2007; Santos et al., 2008).

4.3. Nutrient Speciation and N:P Ratio

Dissolved inorganic nitrogen (DIN) species (NH_4^+, NO_2^-, and NO_3^-) are variable in different water patterns due to their different origins and biogeochemical reactions (Figure 10a). In all the mixing end-members

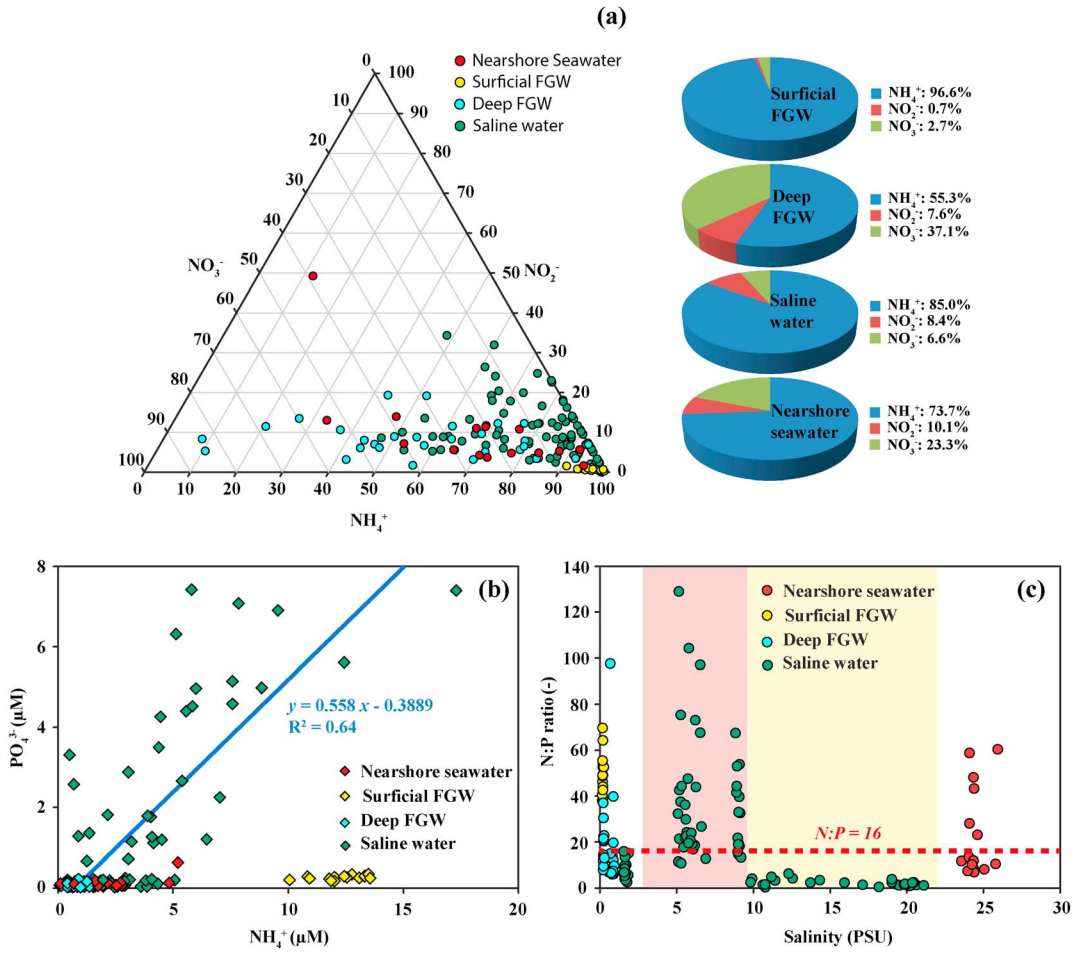

Figure 10. (a) The ternary diagram and pie chart illustrating the percentage of different dissolved inorganic nitrogen species for different water patterns, (b) the relationship between NH_4^+ and PO_4^{3-}, and (c) the relationship between salinity and N:P ratio.

(surficial FGW, deep FGW, and nearshore seawater), NH_4^+ is the most while NO_2^- is the least abundant DIN species (Table 1). However, the proportion of NH_4^+, NO_2^-, and NO_3^- in the three water mixing end-members varies greatly. In surficial FGW, the average percentage of NH_4^+ is 96.5% (ranges from 93.7% to 99.7%), and NO_2^- only accounts for 0.70% (ranges from 0.009% to 1.5%) of DIN. The percentage of NO_3^- ranges from 0.007% to 5.5%, with an average value of 2.61%. In deep FGW, the percentage of NH_4^+ is much lower than in surficial FGW (55.3% versus 96.5%). The percentage of NO_2^- is much higher in deep FGW than in surficial FGW (7.6% versus 0.70%). The proportion of NO_3^- in deep FGW is about 10 times of that in surficial FGW (37.1% versus 2.70%). The fraction of the three components of DIN in nearshore seawater is similar to that in deep groundwater with 73.7% NH_4^+, 7.3% NO_2^-, and 19.0% NO_3^-. Similar to the DIN composition in three mixing end-members mentioned above, accounting for 85.0% of DIN, NH_4^+ is the most abundant DIN species in saline water. However, NO_2^- and NO_3^- have a similar proportion (8.4% versus 6.6%) in saline water, while NO_3^- proportion in the three mixing end-members is several times larger than NO_2^-. This dissimilarity indicates that biogeochemical reactions such as NTR and DNRA that transform NH_4^+ or NO_3^- to NO_2^- are intensive in saline water.

The relationship between major DIN species (NH_4^+) and DIP species (PO_4^{3-}) is presented in Figure 10b. The high correlation between NH_4^+ and PO_4^{3-} in saline water directly proves the same sources of the two ions, that is, REM of organic matters. Theoretically, if all NH_4^+ and PO_4^{3-} in saline water is assumed transformed from REM of organic matters, the slope of fitting line between PO_4^{3-} and NH_4^+ scatters should be around 1/16 (0.0625) according to the N:P ratio of organic matters (Redfield ratio: C:N:P = 106:16:1). However, the

actual slope of fitting line (0.558) is much greater than 1/16, indicating a significant NH_4^+ loss via NTR in saline water. Furthermore, NH_4^+ and PO_4^{3-} scatters in surficial FGW are far away from other scatters in saline water, deep FGW, and nearshore seawater. This also demonstrates different sources of NH_4^+ in surficial FGW and other water patterns. Very high N:P ratio (average value of 49.6) in surficial FGW also confirms that NH_4^+ enriched in surficial FGW is from the external source instead of REM of local organic matters. N:P ratio in deep FGW is ~ 18 (Table 1), which is highly identical to the Redfield ratio (16). The N:P ratio variation in deep FGW is mainly influenced by the interaction between solid and liquid phase such as the adsorption of NH_4^+ onto clay, the adsorption of PO_4^{3-} onto iron oxides, and biogeochemical reactions that remove DIN such as DNTR. The N:P ratio in nearshore seawater is about 23 (Table 1), which is slightly larger than the Redfield ratio (16), which characterizes that the primary productivity of phytoplankton in Tolo Harbour is limited by the supply of DIP. The result is consistent with the previous SGD research (Luo et al., 2014; Luo & Jiao, 2016). The variation of N:P ratio in nearshore seawater is attributed to the discharge of groundwater with different N:P ratios and also the biochemical reactions in seawater. The N:P ratio in saline water can be classified into three parts according to salinity and N:P ratio values (Figure 10c). Saline water with small salinity ($<$ ~ 5 psu) has a N:P ratio (~ 8.4) smaller than Redfield ratio (16) due to N removal by DNTR. The N:P ratio (~ 37) in saline water with salinity between 5 to 10 psu is much higher than the Redfield ratio (16) (Figure 10c), which indicates a low N removal rate and high intensity of PO_4^{3-} adsorption onto iron oxides. Saline water with such N:P ratio configuration is from L3-3, L3-4, and L3-5. At these locations, the organic matters are limited to support DNTR. Furthermore, the location of sampling tubes (L3-3, L3-4, and L3-5) is the pending location of "iron curtain" (Charette & Sholkovitz, 2002; Spiteri et al., 2006) in the intertidal aquifer by comparing with the iron curtain location and associated salinity configuration in the study of McAllister et al. (2015). The N:P ratios (~2) in saline water with the salinity $>$ ~ 10 psu is smaller than the Redfield ratio (16) (Figure 10c), which indicates an intensive removal process of N in this area. The saline water with the salinity $>$ ~ 10 psu is from near-surface area (L2-1 and L3-1), where oxygen and organic matter availabilities are large. Abundant oxygen and organic matters would strengthen N removal processes such as DNTR. Furthermore, in near-surface area, saline water is mainly from the infiltration of nearshore seawater with a low Fe^{2+} concentration. Therefore, the adsorption of PO_4^{3-} onto iron oxides is unlikely to occur in near-surface area. As a result, a low N:P ratio is formed in near-surface area. The discharge of saline water with high P concentration in near-surface area is the major DIP source of seawater, which can strengthen the phytoplankton primary productivity in Tolo Harbour.

4.4. Nutrient Flux

The nutrient flux can be calculated by multiplying flow velocity and porosity to the integrated concentration of each nutrient species at L1, L2, and L3, which can be described as follows (Couturier et al., 2016; Gonneea & Charette, 2014):

$$F_i = v \cdot \int_0^z C_i(z)\mathrm{d}z, \quad (1)$$

where F_i is the flux of nutrient species i, C_i is the concentration of nutrient species i, which is a function of depth, z. According to water level data at this sampling transection, the horizontal velocity at shallow aquifer is calculated to be 0.18 ± 0.01 m/d according to Darcy's law.

Applying equation (1) to nutrient flux calculation, the fluxes of NH_4^+, NO_3^-, NO_2^-, and PO_4^{3-} at sampling sites L1, L2, and L3 at each SR are presented in Table 2. During the sampling period, fluxes of NH_4^+, NO_2^-, NO_3^-, and PO_4^{3-} at sampling site L1 are 2007.37, 24.98, 107.12, and 50.17 mmol m^{-1} yr^{-1}, respectively. At L2, the flux of NH_4^+ decreases to 286.05 mmol m^{-1} yr^{-1} while the PO_4^{3-} increases to 104.45 mmol m^{-1} yr^{-1}, and two other nitrogen species (NO_3^- and NO_2^-) are comparable to L1 with fluxes of 37.49 and 116.55 mmol m^{-1} yr^{-1}, respectively. Therefore, the net production of PO_4^{3-} in the aquifer between L1 and L2 is 54.27 mmol m^{-1} yr^{-1}, while net loss of NH_4^+ is 1721.32 mmol m^{-1} yr^{-1}. At L3, calculated fluxes of NH_4^+, NO_3^-, NO_2^-, and PO_4^{3-} are 805.99, 78.01, 47.77, and 360.64 mmol m^{-1} yr^{-1}, respectively. When water flows from L2 to L3, NH_4^+ in water is enriched with a net production of 519.94 mmol m^{-1} yr^{-1}. The other two enriched nutrient species are NO_2^- and PO_4^{3-} with net production rates of 40.52 and 256.19 mmol m^{-1} yr^{-1}, respectively. NO_3^- in water is depleted with a net consumption rate of 68.78 mmol m^{-1} yr^{-1}.

4.5. Biogeochemical Reactions

Biogeochemical reactions that produce PO_4^{3-} from organic matters are REM and DNTR. The net removal of NH_4^+ should be the processes of coupled NTR-DNTR (Marchant et al., 2016), or coupled NTR-ANAM. Some

Table 2
The Nutrient Fluxes of Each Sampling Sites at Sampling Rounds With Different Tidal Levels

	L1 (mmol m^{-1} yr^{-1})					L2 (mmol m^{-1} yr^{-1})					L3 (mmol m^{-1} yr^{-1})				
SRs	NH_4^+	NO_2^-	NO_3^-	PO_4^{3-}	O_2	NH_4^+	NO_2^-	NO_3^-	PO_4^{3-}	O_2	NH_4^+	NO_2^-	NO_3^-	PO_4^{3-}	O_2
1	1753.40	6.46	40.79	55.03	13567.05	98.88	19.87	53.40	182.07	3043.758	676.87	35.58	28.50	352.65	9827.283
2	1819.63	33.64	109.32	49.93	18691.65	242.27	50.37	215.60	126.60	5661.492	593.01	60.05	75.55	304.03	7319.391
3	2068.24	22.92	154.20	64.96	15028.88	134.19	50.79	172.18	83.08	5892.469	595.44	34.24	95.54	237.54	6386.245
4	2142.35	32.06	95.19	50.14	16063.65	362.01	29.89	81.22	71.89	7139.742	711.63	181.20	148.41	423.39	6645.966
5	1987.82	16.82	35.16	56.92	19512.9	340.65	38.43	43.81	110.03	9973.055	528.59	43.59	1.65	289.48	11939.95
6	2154.96	23.65	169.30	55.56	17262.68	379.91	21.19	132.24	149.52	11523.16	886.79	45.96	76.89	465.07	9738.998
7	1976.78	37.11	89.95	45.20	10741.95	208.43	35.79	98.77	143.64	8479.406	720.66	35.19	27.00	472.63	8725.781
8	2038.80	17.87	170.03	36.79	18018.23	352.48	23.98	143.36	105.23	8407.547	570.47	54.76	19.45	493.11	6354.422
9	2199.11	43.10	296.49	60.76	20596.95	433.29	53.05	250.56	82.40	8417.813	789.02	64.75	10.72	305.94	8255.616
10	2244.31	44.88	119.56	68.49	18133.2	473.04	68.99	119.98	81.37	6472.477	696.68	97.30	19.84	345.31	12206.85
11	2048.26	26.28	114.21	48.88	11743.88	336.38	38.76	169.64	78.53	3464.648	976.73	197.76	103.55	346.13	6606.956
12	1639.35	19.45	144.91	35.16	15455.93	294.83	30.39	126.37	44.59	5071.219	869.77	119.46	73.38	166.97	4705.763
13	1992.55	21.55	31.43	49.62	11793.15	156.69	43.85	46.58	78.08	3161.813	827.06	90.70	31.39	317.47	5211.858
14	1877.44	8.41	16.45	32.06	15111	182.32	38.93	47.32	153.18	6056.719	1444.09	56.27	0.22	503.22	8105.738
15	2167.57	20.50	19.76	43.10	15258.83	295.32	18.07	47.21	76.51	5948.93	1202.97	53.38	4.48	386.67	7609.908
Avg.	2007.37	24.98	107.12	50.17	15798.66	286.05	37.49	116.55	104.45	6580.95	805.99	78.01	47.77	360.64	7976.05

studies indicate that ANAM can contribute a large proportion in NH_4^+ removal in sediments with low content of organic matter (Gao et al., 2009; Marchant et al., 2014; Rao et al., 2008), however, in a sandy beach with high content of organic matters in this study, DNTR is predominant over ANAM (Canion et al., 2014). According to Table S2, the groundwater sometimes is in oxic condition (> 20 μM) or suboxic condition (between detection limit and 20 μM). Because the growth of the ANAM bacteria was reversibly inhibited even by DO level even below 0.5% air saturation (~ 1.25 μM) (Kuenen, 2008), in the system with such a high concentration of DO (> 6 μM) in this study (Table S2), the removal of NH_4^+ is hardly due to ANAM. Therefore, biogeochemical reactions possibly responsible for the production and removal of nutrients are coupled REM + NTR + DNTR. The biogeochemical reactions are given in Table 3. According to biogeochemical reactions and combination scenarios, the production and removal rates of nutrient species (NH_4^+, NO_2^-, NO_3^-, and PO_4^{3-}) are calculated and presented in Table 4.

4.5.1. REM + NTR + DNTR

In the aquifer between L1 and L2, external NH_4^+ input (2007.37 mmol m^{-1} yr^{-1}) from L1 which contributes 80.2% of NH_4^+ is the major source while the REM of organic matter (496.19 mmol m^{-1} yr^{-1}) only accounts for 19.8%. The reaction leading to the depletion of NH_4^+ is NTR1 that consumes NH_4^+ and produces NO_2^- simultaneously with a rate of 2217.51 mmol m^{-1} yr^{-1}, and accounting for 88.6% of total NH_4^+ sinks. The produced NO_2^- is continuously oxidized to NO_3^- via NTR2 with a rate of 2205.00 mmol m^{-1} yr^{-1}. For PO_4^{3-}, 48.0% is from external input (50.17 mmol m^{-1} yr^{-1}), 29.7% is from REM of organic matter (31.01 mmol m^{-1} yr^{-1}), and 22.3% is from DNTR (23.26 mmol m^{-1} yr^{-1}). The total consumption rate of O_2 in the aquifer between L1 and L2 is 7716.01 mmol m^{-1} yr^{-1}, in which O_2 consumption via REM, NTR1, and NTR2 accounts for 42.6%, 43.1%, and 14.3%, respectively. The total O_2 consumption rate is very close to the net loss of O_2 in the aquifer (7716.01 versus 9217.71 mmol m^{-1} yr^{-1}), which indicates that the oxygen supply in this aquifer is mainly from the oxic surficial FGW and it is believed that there are some other reactions consume the oxygen besides the REM and NTR.

Table 3
The Equations of the Biogeochemical Reactions in the Aquifer

Name	Reaction
Remineralization of organic matter (REM)	$(CH_2O)_{106}(NH_3)_{16}H_3PO_4 + 106O_2 + 16H^+ \rightarrow 106CO_2 + 16NH_4^+ + 106H_2O + H_3PO_4$
Nitrification (NTR1)	$NH_4^+ + 1.5O_2 \rightarrow NO_2^- + H_2O + 2H^+$
Nitrification (NTR2)	$NO_2^- + 0.5O_2 \rightarrow NO_3^-$
Denitrification (DNTR)	$(CH_2O)_{106}(NH_3)_{16}H_3PO_4 + 94.4NO_3^- + 94.4H^+ \rightarrow 106CO_2 + 55.2N_2 + H_3PO_4 + 177.2H_2O$
Anammox (ANAM)	$NH_4^+ + NO_2^- \rightarrow N_2 + 2H_2O$

Table 4
The Budget of Each Nutrient Species in Different Biogeochemical Reactions (the Positive Value Means Production While the Negative Value Means Consumption)

	L1-L2 (mmol m^{-1} yr^{-1})					L2-L3 (mmol m^{-1} yr^{-1})				
	NH_4^+	NO_2^-	NO_3^-	PO_4^{3-}	O_2	NH_4^+	NO_2^-	NO_3^-	PO_4^{3-}	O_2
Net	−1721.32	12.51	9.43	54.27	−9217.7	519.94	40.52	−68.78	256.19	1395.1
REM	496.19	0	0	31.01	−3287.3	3576.23	0	0	223.51	−23692.6
NTR1	−2217.51	2217.51	0	0	−3326.3	−3056.29	3056.29	0	0	−4584.4
NTR2	0	−2205	2205	0	−1102.5	0	−3015.77	3015.77	0	−1507.9
DNTR	0	0	−2195.57	23.26	0	0	0	−3084.56	32.68	0

In the aquifer from L2 to L3, REM of organic matters contributes majority of NH_4^+ (92.6%) with a rate of 3576.23 mmol m^{-1} yr^{-1}. NTR1 consumes 79.1% (3056.29 mmol m^{-1} yr^{-1}) of total NH_4^+ inputs (both external input from L2 and produced via REM of organic matter) and is a major sink. The 98.7% of the produced NO_2^- via NTR1 (3056.29 mmol m^{-1} yr^{-1}) is transformed to NO_2^- with a rate of 3015.77 mmol m^{-1} yr^{-1}. The reaction rate of DNTR is 3084.56 mmol m^{-1} yr^{-1}, and DNTR is the major sink of NO_3^-. External inputs, DNTR, and REM of organic matter contribute 29.0% (104.45 mmol m^{-1} yr^{-1}), 9.0% (32.68 mmol m^{-1} yr^{-1}), and 62.0% (223.51 mmol m^{-1} yr^{-1}) of the PO_4^{3-} input source, respectively. As for the oxygen consumption, REM holds an oxygen consumption rate of 23692 mmol m^{-1} yr^{-1} that accounts for 79.5% of the total oxygen consumption. The oxygen consumption rates via NTR1 (4584.44 mmol m^{-1} yr^{-1}) and NTR2 (1507.89 mmol m^{-1} yr^{-1}) account for the rest 15.4% and 5.1%, respectively. It is worth noting that the net DO (output from L3 subtract input from L2) is positive even though the oxygen consumption via REM and NTR is very large, which is because DO in the aquifer from L2 to L3 is supported by the infiltration of high DO nearshore seawater (~ 140 μM).

Compare aquifer from L1 to L2 with aquifer from L2 to L3, intensities of REM of organic matter, NTR, and DNTR in aquifer from L2 to L3 are much larger than that in aquifer from L1 to L2. The higher intensity of REM in aquifer from L2 to L3 is caused by more organic matter inputs and oxygen supply via seawater infiltration. The higher rates of EM of organic matters are the causative of the high rates of NTR and DNTR in this aquifer because the external input of NH_4^+ in the aquifer from L2 to L3 is less than that in the aquifer from L1 to L2. In addition, the higher production (REM) and removal (NTR) rates of NH_4^+ result in a higher oxygen consumption rates in the aquifer from L2 to L3 than in the aquifer from L1 to L2 (7716.01 versus −29784.88 mmol m^{-1} y^{-1}). For P species, the contribution of production via REM of organic matter is much larger in aquifer from L2 to L3 than in the aquifer from L1 to L2. These differences in the production of nutrients and consumption of oxygen in the two aquifers suggest that the different degree of organic matters and oxygen input via the infiltration of seawater during the high tide is the main controlling factor of biogeochemical transformation of nutrients in the aquifer.

4.5.2. Nutrients Loss and Production

Regarding the aquifer between L1 and L3 as the whole CGMZ (20 m), NH_4^+ loss in the aquifer is 5273.80 mmol m^{-1} yr^{-1} via NTR. The 77% of NH_4^+ loss in the aquifer is supported by REM of organic matter. The production rate of PO_4^{3-} is 310.46 mmol m^{-1} yr^{-1}, and within which more than 80% is from REM of organic matter, and less than 20% is from DNTR. The oxygen consumed by REM of organic matters is 2.56 times that by NTR in CGMZ. The input and output of nutrients flux to CGMZ and the removal and production of nutrients via biogeochemical reactions in the aquifer are all illustrated in Figure 11.

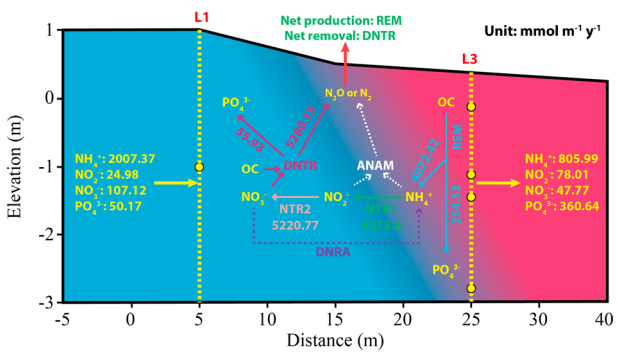

Figure 11. The schematic diagram of nutrients flux, production, and removal of nutrients in CGMZ.

Extrapolating the consumption or production rate to the whole Tolo Harbour with 82 km coastline, total annual NH_4^+ loss via NTR is about 4.32×10^5 mol in the CGMZ, and total annual PO_4^{3-} production is about 2.55×10^4 mol. It worth noting that the calculated value could be underestimated as it is based on the assumption that Tolo Harbour is surrounded by 20 m wide beach. Thus, the value calculated in this section represents the minimum value for the entire Tolo Harbour. If the whole Tolo Harbour (including the subtidal and

Table 5
The Geochemical Reaction Rates in Costal Sediments, Unit: mmol m^{-2} d^{-1}

Location	Type of sediments	NTR	DNTR	O_2 consumption	References
Tolo Harbour	Intertidal upper flat (0–3 m)	> 0.72	> 0.73	> 5.14	This Study
German Bight	Subtidal (0–5 cm)	0.21–2.98	0.52–2.28	26.3–49.6	Marchant et al. (2016)
Spiekeroog Island, Wadden Sea	Intertidal upper flat (0–15 cm)		31.14–82.08	975.6–1652.4	Marchant et al. (2014)
East Frisian, Wadden Sea	Intertidal (0–10 cm)		3.5–7.2		Gao et al. (2012)
Janssand, Wadden Sea	Intertidal (0–6 cm)		> 4.56		Gao et al. (2009)
Sapelo Island, Georgia	Intertidal Aquifer (1–5 m)		10		Schutte et al. (2015)
Texel, Wadden Sea	Intertidal (1–2 cm)		0.02–1.01		Kieskamp et al. (1991)
Southern North Sea	Seafloor (0–5 cm)		0.14–0.21		Lohse et al. (1996)
North Pacific	Continental shelf (0–8 cm)		0.21–0.29		Devol (1991)
Washington State Shelf	Continental shelf		3.1992		
Bering, Chukchi, and Beaurfort Seas	Seafloor (0–25 cm)		0.8064		Devol et al. (1997)
Mid-Altantic Bight	Continental shelf		1.6512		Laursen and Seitzinger (2002)
North Sea, off Belgian Coasts	Seafloor (0–30 cm)	0.9–16.6	0–7.25		Billen (1978)
Baltic Sea	Seafloor		0–1		Shaffer and Rönner (1984)
Baltic Sea	Beach and Seafloor		0.012–0.69		Deutsch et al. (2010)
Northern Baltic Sea	Seafloor (0–10 cm)		0–3		Tuominen et al. (1998)
Gulf of Finland	Seafloor (0–10 cm)		0.072–0.64		
Aarhus Bay	Seafloor (5–9 cm)		0.29–0.5		Nielsen and Glud (1996)
North-West Africa	Continental shelf		0.8–9.0		Sokoll et al. (2016)
South Atlantic Bight	Continental shelf		0.25–1.5		Rao et al. (2007)
Australian Coast	Lagoon floor (0–5 cm)		0–8.1		Santos et al. (2012)
Thames Estuary	Intertidal (0–2 cm)		0.3–1.28		Trimmer et al. (2003)
Arctic Marine Sediments	Subtidal (0–4 cm)	0.03–0.46	0.03–0.27		Rysgaard et al. (2004)
Logan River, Australia	Mangrove sediments		3.38–70.86		Meyer et al. (2005)
Yodo Estuary Japan	Intertidal (0–2 cm)		8.76–36.8		Amano et al. (2007)
Heron Island, Australia	Subtidal (0–10 m)		0.1–5.9		Huettel et al. (2014)
All over the world			0–30.2		Joye and Anderson (2008)

bottom area) is considered, the calculated areal rates of REM, NTR, DNTR, and the consumption of O_2 are 0.56 mmol N m^{-2} d^{-1}, 0.72 mmol N m^{-2} d^{-1}, 0.73 mmol N m^{-2} d^{-1}, and 5.14 mmol m^{-2} d^{-1}, respectively. Those calculated values agree well with the values in literature, which are listed in Table 5. Extrapolating the consumption or production rates to the whole Tolo Harbour with an area of 50 km^2, the annual NH_4^+ inputs via REM is about 1.02×10^7 mol while the annual NH_4^+ loss via NTR is about 1.32×10^7 mol. The annual PO_4^{3-} production is about 7.76×10^5 mol. This value is comparable to the DIP inputs via SGD estimated by Luo and Jiao (2016), which indicates that the REM of organic matter is the major input of DIP in Tolo Harbour.

5. Conclusions

In this study, the intensive measurements of nutrients in CGMZ at different tidal stages successfully grasp the fluctuated temporal variation of nutrients with tidal oscillation. The mechanism of the variation under tidal fluctuation and the biogeochemical reactions in the aquifer are revealed by both quantitative and qualitative analysis. The results show that tidal pumping influences REM of organic matters through controlling inputs of the organic matter. Subsequently, tidal pumping affects the configuration and fluctuation of NH_4^+ and PO_4^{3-} in the aquifer. Therefore, NH_4^+ and PO_4^{3-} are positively correlated with salinity and have negative correlations with ORP. N:P ratio results show that the adsorption of PO_4^{3-} onto iron oxides occurs at the deep transition zone with a salinity between 5 to 10 psu, and the intensive N-loss occurs at near surface area with a salinity between 10 and 25 psu. REM of organic matters, accounting for >65% of the total NH_4^+ input to groundwater, is the major NH_4^+ source. As the major PO_4^{3-} source, REM + DNTR produces ~ 86% of the total PO_4^{3-}. NTR is the major sink of NH_4^+ that consumes ~ 87% of the total NH_4^+. The minimum annual NH_4^+ loss in CGMZ is estimated to be 4.32×10^5 mol for NTR, and the minimum annual PO_4^{3-} production in CGMZ is estimated to be 2.55×10^4 mol. As for the whole Tolo Harbour, the annual NH_4^+ input via REM is estimated to be 1.02×10^7 mol. Annually, NH_4^+ loss via NTR is estimated to be 1.32×10^7 mol, while the PO_4^{3-} production is about 7.76×10^5 mol.

Acknowledgments
All the data reported in this study are listed in the supporting information. This study was supported by the grants from the National Natural Science Foundation of China (41372261) and Research Grants Council of Hong Kong (HKU 7028/06P). The authors would like to thank the technicians Ho and Chio for their help of installation of sampler and the field works. The assistances of Jin, Hua, Feng, and Cheng when sampling in the field and postprocessing of water sample are also appreciated.

References

Abarca, E., Karam, H., Hemond, H. F., & Harvey, C. F. (2013). Transient groundwater dynamics in a coastal aquifer: The effects of tides, the lunar cycle, and the beach profile. *Water Resources Research*, *49*, 2473–2488. https://doi.org/10.1002/wrcr.20075

Amano, T., Yoshinaga, I., Okada, K., Yamagishi, T., Ueda, S., Obuchi, A., … Suwa, Y. (2007). Detection of anammox activity and diversity of anammox bacteria-related 16S rRNA genes in coastal marine sediment in Japan. *Microbes and Environments*, *22*, 232–242. https://doi.org/10.1264/jsme2.22.232

Amoozegar, A. (1989). A compact constant-head permeameter for measuring saturated hydraulic conductivity of the vadose zone. *Soil Science Society of America Journal*, *53*(5). https://doi.org/10.2136/sssaj1989.03615995005300050009x

Beck, A. J., Cochran, J. K., & Sanudo-Wilhelmy, S. A. (2010). The distribution and speciation of dissolved trace metals in a shallow subterranean estuary. *Marine Chemistry*, *121*, 145–156. https://doi.org/10.1016/j.marchem.2010.04.003

Billen, G. (1978). A budget of nitrogen recycling in North Sea sediments off the Belgian coast. *Estuarine and Coastal Marine Science*, *7*(2), 127–146. https://doi.org/10.1016/0302-3524(78)90070-1

Burnett, W. C., Aggarwal, P. K., Aureli, A., Bokuniewicz, H., Cable, J. E., Charette, M. A., … Turner, J. V. (2006). Quantifying submarine groundwater discharge in the coastal zone via multiple methods. *Science of the Total Environment*, *367*, 498–543. https://doi.org/10.1016/j.scitotenv.2006.05.009

Burnett, W. C., Wattayakorn, G., Taniguchi, M., Dulaiova, H., Sojisuporn, P., Rungsupa, S., & Ishitobi, T. (2007). Groundwater-derived nutrient inputs to the Upper Gulf of Thailand. *Continental Shelf Research*, *27*, 176–190. https://doi.org/10.1016/j.csr.2006.09.006

Cable, J. E., Burnett, W. C., Chanton, J. P., & Weatherly, G. L. (1996). Estimating groundwater discharge into the northeastern Gulf of Mexico using radon-222. *Earth and Planetary Science Letters*, *144*(3-4), 591–604. https://doi.org/10.1016/S0012-821X(96)00173-2

Canion, A., Kostka, J. E., Gihring, T. M., Huettel, M., van Beusekom, J. E. E., Gao, H., … Kuypers, M. M. M. (2014). Temperature response of denitrification and anammox reveals the adaptation of microbial communities to in situ temperatures in permeable marine sediments that span 50? in latitude. *Biogeosciences*, *11*(2), 309–320. https://doi.org/10.5194/bg-11-309-2014

Chan, B., Chan, L. Y., Chan, S. C., Cheung, C. M., Kwan, M., Lam, M. Y., … Yiu, Y. N. (1995). Shore Zone Fandelta Deposition At Ting Kok, Plover Cove. Hong Kong Geologist, 5.

Charette, M. A., & Sholkovitz, E. R. (2002). Oxidative precipitation of groundwater-derived ferrous iron in the subterranean estuary of a coastal bay. *Geophysical Research Letters*, *29*(10), 85-1–85-4. https://doi.org/10.1029/2001GL014512

Choi, H.-Y. (2001). Oceanographic condition of the coastal area between Narodo Is. and Solido Is. in the Southern Sea of Korea and its relation to the disappearance of red-tide observed in summer 1998. *The Sea*, *6*(2), 49–62.

Couturier, M., Tommi-Morin, G., Sirois, M., Rao, A., Nozais, C., & Chaillou, G. (2016). Nitrogen transformations along a shallow subterranean estuary. *Biogeosciences*, *14*(13), 3321–3336. https://doi.org/10.5194/bg-2016-535

Craig, H. (1961). Isotopic variations in meteoric waters. *Science*, *133*(3465), 1702–1703. https://doi.org/10.1126/science.133.3465.1702

Deutsch, B., Forster, S., Wilhelm, M., Dippner, J. W., & Voss, M. (2010). Denitrification in sediments as a major nitrogen sink in the Baltic Sea: An extrapolation using sediment characteristics. *Biogeosciences*, *7*, 3259–3271. https://doi.org/10.5194/bg-7-3259-2010

Devol, A. H. (1991). Direct measurement of nitrogen gas fluxes from continental shelf sediments. *Nature*, *349*(6307), 319–321. https://doi.org/10.1038/349319a0

Devol, A. H., Codispoti, L. A., & Christensen, J. P. (1997). Summer and winter denitrification rates in western Arctic shelf sediments. *Continental Shelf Research*, *17*(9), 1029–1050. https://doi.org/10.1016/S0278-4343(97)00003-4

Fetter, C. W. (2000). *Applied Hydrogeology*. NJ: Prentice Hall.

Gao, H., Schreiber, F., Collins, G., Jensen, M. M., Svitlica, O., Kostka, J. E., … Kuypers, M. M. (2009). Aerobic denitrification in permeable Wadden Sea sediments. *The ISME Journal*, *4*, 417–426. https://doi.org/10.1038/ismej.2009.127

Gao, H., Matyka, M., Liu, B., Khalili, A., Kostka, J. E., Collins, G., … Kuypers, M. M. M. (2012). Intensive and extensive nitrogen loss from intertidal permeable sediments of the Wadden Sea. *Limnology and Oceanography*, *57*(1), 185–198. https://doi.org/10.4319/lo.2012.57.1.0185

Gonneea, M. E., & Charette, M. A. (2014). Hydrologic controls on nutrient cycling in an unconfined coastal aquifer. *Environmental Science & Technology*, *48*(24), 14178–14185. https://doi.org/10.1021/es503313t

Heiss, J. W., & Michael, H. A. (2014). Saltwater-freshwater mixing dynamics in a sandy beach aquifer over tidal, spring-neap, and seasonal cycles. *Water Resources Research*, *50*, 6747–6766. https://doi.org/10.1002/2014WR015574

Huettel, M., Berg, P., & Kostka, J. E. (2014). Benthic exchange and biogeochemical cycling in permeable sediments. *Annual Review of Marine Science*, *6*(1), 23–51. https://doi.org/10.1146/annurev-marine-051413-012706

Hulth, S., Aller, R. C., Canfield, D. E., Dalsgaard, T., Engström, P., Gilbert, F., … Thamdrup, B. (2005). Nitrogen removal in marine environments: Recent findings and future research challenges. *Marine Chemistry*, *94*, 125–145. https://doi.org/10.1016/j.marchem.2004.07.013

Hwang, D.-W., Kim, G., Lee, Y.-W., & Yang, H.-S. (2005). Estimating submarine inputs of groundwater and nutrients to a coastal bay using radium isotopes. *Marine Chemistry*, *96*, 61–71. https://doi.org/10.1016/j.marchem.2004.11.002

Hwang, D., Lee, Y.-W., & Kim, G. (2005). Large submarine groundwater discharge and benthic eutrophication in Bangdu Bay on volcanic Jeju Island, Korea. *Limnology and Oceanography*, *50*, 1393–1403. https://doi.org/10.4319/lo.2005.50.5.1393

Johannes, R. (1980). Ecological significance of the submarine discharge of groundwater. *Marine Ecology Progress Series*, *3*(4), 365–373. https://doi.org/10.3354/meps003365

Joye, S. B., & Anderson, I. C. (2008). *Chapter 19 - Nitrogen cycling in Coastal Sediments, Nitrogen in the Marine Environment*, (2nd ed.pp. 867–915). San Diego: Academic Press.

Kieskamp, W. M., Lohse, L., Epping, E., & Helder, W. (1991). Seasonal variation in denitrification rates and nitrous oxide fluxes in intertidal sediments of the western Wadden Sea. *Marine Ecology Progress Series*, *72*(1), 145–151. https://doi.org/10.3354/meps072145

Kroeger, K. D., & Charette, M. A. (2008). Nitrogen biogeochemistry of submarine groundwater discharge. *Limnology and Oceanography*, *53*, 1025–1039. https://doi.org/10.4319/lo.2008.53.3.1025

Kroeger, K. D., Swarzenski, P. W., Greenwood, W. J., & Reich, C. D. (2007). Submarine groundwater discharge to Tampa Bay: Nutrient fluxes and biogeochemistry of the coastal aquifer. *Marine Chemistry*, *104*, 85–97. https://doi.org/10.1016/j.marchem.2006.10.012

Kuenen, J. G. (2008). Anammox bacteria: From discovery to application. *Nature Reviews. Microbiology*, *6*, 320–326. https://doi.org/10.1038/nrmicro1857

Lapointe, B. E. (1997). Nutrient thresholds for bottom-up control of macroalgal blooms on coral reefs in Jamaica and southeast Florida. *Limnology and Oceanography*, *42*(5part2), 1119–1131. https://doi.org/10.4319/lo.1997.42.5_part_2.1119

Laroche, J., Nuzzi, R., Waters, R., Wyman, K., Falkowski, P., & Wallace, D. (1997). Brown tide blooms in Long Island's coastal waters linked to interannual variability in groundwater flow. *Global Change Biology*, *3*(5), 397–410. https://doi.org/10.1046/j.1365-2486.1997.00117.x

Laursen, A. E., & Seitzinger, S. P. (2002). The role of denitrification in nitrogen removal and carbon mineralization in mid-Atlantic Bight sediments. *Continental Shelf Research*, *22*(9), 1397–1416. https://doi.org/10.1016/S0278-4343(02)00008-0

Lecher, A. L., Chien, C.-T., & Paytan, A. (2016). Submarine groundwater discharge as a source of nutrients to the North Pacific and Arctic coastal ocean. *Marine Chemistry*, *186*(Supplement C), 167–177. https://doi.org/10.1016/j.marchem.2016.09.008

Lee, R. Y., & Joye, S. B. (2006). Seasonal patterns of nitrogen fixation and denitrification in oceanic mangrove habitats. *Marine Ecology Progress Series*, *307*, 127–141. https://doi.org/10.3354/meps307127

Lee, Y.-W., Hwang, D.-W., Kim, G., Lee, W.-C., & Oh, H.-T. (2009). Nutrient inputs from submarine groundwater discharge (SGD) in Masan Bay, an embayment surrounded by heavily industrialized cities, Korea. *Science of the Total Environment*, *407*, 3181–3188. https://doi.org/10.1016/j.scitotenv.2008.04.013

Lee, Y. W., Kim, G., Lim, W. A., & Hwang, D. W. (2010). A relationship between submarine groundwater-borne nutrients traced by Ra isotopes and the intensity of dinoflagellate red-tides occurring in the southern sea of Korea. *Limnology and Oceanography*, *55*, 1–10. https://doi.org/10.4319/lo.2010.55.1.0001

Lee, C. M., Jiao, J. J., Luo, X., & Moore, W. S. (2012). Estimation of submarine groundwater discharge and associated nutrient fluxes in Tolo Harbour, Hong Kong. *The Science of the Total Environment*, *433*, 427–433. https://doi.org/10.1016/j.scitotenv.2012.06.073

Li, H., Sun, P., Chen, S., Xia, Y., & Liu, S. (2010). A falling-head method for measuring intertidal sediment hydraulic conductivity. *Ground Water*, *48*, 206–211. https://doi.org/10.1111/j.1745-6584.2009.00638.x

Li, Y., Zhang, M., Wang, S., Li, Z., & Wang, F. (2012). Stable isotope in precipitation in China: A review. *Sciences in Cold and Arid Regions*, *4*, 0083–0090.

Lie, A. A. Y., Wong, C. K., Lam, J. Y. C., Liu, J. H., & Yung, Y. K. (2011). Changes in the nutrient ratios and phytoplankton community after declines in nutrient concentrations in a semi-enclosed bay in Hong Kong. *Marine Environmental Research*, *71*, 178–188. https://doi.org/10.1016/j.marenvres.2011.01.001

Liu, Y., Jiao, J. J., & Liang, W. (2017). Tidal Fluctuation Influenced Physicochemical Parameter Dynamics in Coastal Groundwater Mixing Zone. *Estuaries and Coasts*. https://doi.org/10.1007/s12237-017-0335-x

Liu, Y., Jiao, J. J., Liang, W., & Kuang, X. (2017). Hydrogeochemical characteristics in coastal groundwater mixing zone. *Applied Geochemistry*, *85*(Part A), 49–60. https://doi.org/10.1016/j.apgeochem.2017.09.002

Liu, J. A., Su, N., Wang, X. L., & Du, J. Z. (2017). Submarine groundwater discharge and associated nutrient fluxes into the Southern Yellow Sea: A case study for semi-enclosed and oligotrophic seas-implication for green tide bloom. *Journal of Geophysical Research: Oceans*, *122*, 139–152. https://doi.org/10.1002/2016jc012282

Lohse, L., Kloosterhuis, H. T., van Raaphorst, W., & Helder, W. (1996). Denitrification rates as measured by the isotope pairing method and by the acetylene inhibition technique in continental shelf sediments of the North Sea. *Marine Ecology Progress Series*, *132*, 169–179. https://doi.org/10.3354/meps132169

Loveless, A. M., & Oldham, C. E. (2010). Natural attenuation of nitrogen in groundwater discharging through a sandy beach. *Biogeochemistry*, *98*, 75–87. https://doi.org/10.1007/s10533-009-9377-x

Luo, X., & Jiao, J. J. (2016). Submarine groundwater discharge and nutrient loadings in Tolo Harbor, Hong Kong using multiple geotracer-based models, and their implications of red tide outbreaks. *Water Research*, *102*, 11–31. https://doi.org/10.1016/j.watres.2016.06.017

Luo, X., Jiao, J. J., Moore, W. S., & Lee, C. M. (2014). Submarine groundwater discharge estimation in an urbanized embayment in Hong Kong via short-lived radium isotopes and its implication of nutrient loadings and primary production. *Marine Pollution Bulletin*, *82*(1-2), 144–154. https://doi.org/10.1016/j.marpolbul.2014.03.005

Luo, X., Kwok, K. L., Liu, Y., & Jiao, J. (2017). A permanent multilevel monitoring and sampling system in the coastal groundwater mixing zones. *Groundwater*, *55*(4), 577–587. https://doi.org/10.1111/gwat.12510

Magalhães, C. M., Joye, S. B., Moreira, R. M., Wiebe, W. J., & Bordalo, A. A. (2005). Effect of salinity and inorganic nitrogen concentrations on nitrification and denitrification rates in intertidal sediments and rocky biofilms of the Douro River estuary, Portugal. *Water Research*, *39*, 1783–1794. https://doi.org/10.1016/j.watres.2005.03.008

Marchant, H. K., Lavik, G., Holtappels, M., & Kuypers, M. M. M. (2014). The fate of nitrate in intertidal permeable sediments. *PLoS One*, *9*(8), e104517. https://doi.org/10.1371/journal.pone.0104517

Marchant, H. K., Holtappels, M., Lavik, G., Ahmerkamp, S., Winter, C., & Kuypers, M. M. M. (2016). Coupled nitrification–denitrification leads to extensive N loss in subtidal permeable sediments. *Limnology and Oceanography*, *61*(3), 1033–1048. https://doi.org/10.1002/lno.10271

McAllister, S. M., Barnett, J. M., Heiss, J. W., Findlay, A. J., MacDonald, D. J., Dow, C. L., … Chan, C. S. (2015). Dynamic hydrologic and biogeochemical processes drive microbially enhanced iron and sulfur cycling within the intertidal mixing zone of a beach aquifer. *Limnology and Oceanography*, *60*(1), 329–345. https://doi.org/10.1002/lno.10029

Meyer, R. L., Risgaard-Petersen, N., & Allen, D. E. (2005). Correlation between anammox activity and microscale distribution of nitrite in a subtropical mangrove sediment. *Applied and Environmental Microbiology*, *71*, 6142–6149. https://doi.org/10.1128/AEM.71.10.6142-6149.2005

Michael, H. A., Mulligan, A. E., & Harvey, C. F. (2005). Seasonal oscillations in water exchange between aquifers and the coastal ocean. *Nature*, *436*, 1145–1148. https://doi.org/10.1038/nature03935

Moore, W. S. (1996). Large groundwater inputs to coastal waters revealed by 226Ra enrichments. *Nature*, *380*(6575), 612–614. https://doi.org/10.1038/380612a0

Moore, W. S. (2010). The effect of submarine groundwater discharge on the ocean. *Annual Review of Marine Science*, *2*, 59–88. https://doi.org/10.1146/annurev-marine-120308-081019

Morse, J. W., & Morin, J. (2005). Ammonium interaction with coastal marine sediments: Influence of redox conditions on K*. *Marine Chemistry*, *95*, 107–112. https://doi.org/10.1016/j.marchem.2004.08.008

Nielsen, L. P., & Glud, R. N. (1996). Denitrification in a coastal sediment measured in situ by the nitrogen isotope pairing technique applied to a benthic flux chamber. *Marine Ecology Progress Series*, *137*, 181–186. https://doi.org/10.3354/meps137181

Niencheski, L. F. H., Windom, H. L., Moore, W. S., & Jahnke, R. A. (2007). Submarine groundwater discharge of nutrients to the ocean along a coastal lagoon barrier, southern Brazil. *Marine Chemistry*, *106*, 546–561. https://doi.org/10.1016/j.marchem.2007.06.004

Paytan, A., & McLaughlin, K. (2007). The oceanic phosphorus cycle. *Chemical Reviews*, *107*, 563–576. https://doi.org/10.1021/cr0503613

Paytan, A., Shellenbarger, G. G., Street, J. H., Gonneea, M. E., Davis, K., Young, M. B., & Moore, W. S. (2006). Submarine groundwater discharge: An important source of new inorganic nitrogen to coral reef ecosystems. *Limnology and Oceanography*, *51*, 343–348. https://doi.org/10.4319/lo.2006.51.1.0343

Rao, A. M. F., McCarthy, M. J., Gardner, W. S., & Jahnke, R. A. (2007). Respiration and denitrification in permeable continental shelf deposits on the South Atlantic Bight: Rates of carbon and nitrogen cycling from sediment column experiments. *Continental Shelf Research*, *27*, 1801–1819. https://doi.org/10.1016/j.csr.2007.03.001

Rao, A. M. F., McCarthy, M. J., Gardner, W. S., & Jahnke, R. A. (2008). Respiration and denitrification in permeable continental shelf deposits on the South Atlantic Bight: N2:Ar and isotope pairing measurements in sediment column experiments. *Continental Shelf Research*, *28*, 602–613. https://doi.org/10.1016/j.csr.2007.11.007

Robinson, C., Li, L., & Barry, D. A. (2007). Effect of tidal forcing on a subterranean estuary. *Advances in Water Resources*, *30*, 851–865. https://doi.org/10.1016/j.advwatres.2006.07.006

Rodellas, V., Garcia-Orellana, J., Tovar-Sánchez, A., Basterretxea, G., López-Garcia, J. M., Sánchez-Quiles, D., … Masqué, P. (2014). Submarine groundwater discharge as a source of nutrients and trace metals in a Mediterranean Bay (Palma Beach, Balearic Islands). *Marine Chemistry*, *160*, 56–66. https://doi.org/10.1016/j.marchem.2014.01.007

Rouxel, O., Sholkovitz, E., Charette, M., & Edwards, K. J. (2008). Iron isotope fractionation in subterranean estuaries. *Geochimica et Cosmochimica Acta*, *72*, 3413–3430. https://doi.org/10.1016/j.gca.2008.05.001

Rysgaard, S., Glud, R. N., Risgaard-Petersen, N., & Dalsgaard, T. (2004). Denitrification and anammox activity in Arctic marine sediments. *Limnology and Oceanography*, *49*, 1493–1502. https://doi.org/10.4319/lo.2004.49.5.1493

Santoro, A. E. (2010). Microbial nitrogen cycling at the saltwater-freshwater interface. *Hydrogeology Journal*, *18*(1), 187–202. https://doi.org/10.1007/s10040-009-0526-z

Santoro, A. E., Boehm, A. B., & Francis, C. A. (2006). Denitrifier community composition along a nitrate and salinity gradient in a coastal aquifer. *Applied and Environmental Microbiology*, *72*, 2102–2109. https://doi.org/10.1128/AEM.72.3.2102-2109.2006

Santoro, A. E., Francis, C. A., De Sieyes, N. R., & Boehm, A. B. (2008). Shifts in the relative abundance of ammonia-oxidizing bacteria and archaea across physicochemical gradients in a subterranean estuary. *Environmental Microbiology*, *10*, 1068–1079. https://doi.org/10.1111/j.1462-2920.2007.01547.x

Santos, I. R., Burnett, W. C., Chanton, J., Mwashote, B., Suryaputra, I. G. N. A., & Dittmar, T. (2008). Nutrient biogeochemistry in a Gulf of Mexico subterranean estuary and groundwater-derived fluxes to the coastal ocean. *Limnology and Oceanography*, *53*, 705–718. https://doi.org/10.4319/lo.2008.53.2.0705

Santos, I. R., Burnett, W. C., Dittmar, T., Suryaputra, I. G. N. A., & Chanton, J. (2009). Tidal pumping drives nutrient and dissolved organic matter dynamics in a Gulf of Mexico subterranean estuary. *Geochimica et Cosmochimica Acta*, *73*, 1325–1339. https://doi.org/10.1016/j.gca.2008.11.029

Santos, I. R., Eyre, B. D., & Glud, R. N. (2012). Influence of porewater advection on denitrification in carbonate sands: Evidence from repacked sediment column experiments. *Geochimica et Cosmochimica Acta*, *96*, 247–258. https://doi.org/10.1016/j.gca.2012.08.018

Schlesinger, W. H. (2009). On the fate of anthropogenic nitrogen. *Proceedings of the National Academy of Sciences*, *106*(1), 203–208. https://doi.org/10.1073/pnas.0810193105

Schutte, C. A., Joye, S. B., Wilson, A. M., Evans, T., Moore, W. S., & Casciotti, K. (2015). Intense nitrogen cycling in permeable intertidal sediment revealed by a nitrous oxide hot spot. *Global Biogeochemical Cycles*, *29*, 1584–1598. https://doi.org/10.1002/2014GB005052

Shaffer, G., & Rönner, U. (1984). Denitrification in the Baltic proper deep water. Deep Sea research part A. *Oceanographic Research Papers*, *31*(3), 197–220. https://doi.org/10.1016/0198-0149(84)90102-X

Slomp, C. P., & Van Cappellen, P. (2004). Nutrient inputs to the coastal ocean through submarine groundwater discharge: Controls and potential impact. *Journal of Hydrology*, *295*, 64–86. https://doi.org/10.1016/j.jhydrol.2004.02.018

Smith, C. G., & Swarzenski, P. W. (2012). An investigation of submarine groundwater—Borne nutrient fluxes to the west Florida shelf and recurrent harmful algal blooms. *Limnology and Oceanography*, *57*, 471–485. https://doi.org/10.4319/lo.2012.57.2.0471

Sokoll, S., Lavik, G., Sommer, S., Goldhammer, T., Kuypers, M. M. M., & Holtappels, M. (2016). Extensive nitrogen loss from permeable sediments off north-west Africa. *Journal of Geophysical Research: Biogeosciences*, *121*, 1144–1157. https://doi.org/10.1002/2015JG003298

Spiteri, C., Regnier, P., Slomp, C. P., & Charette, M. A. (2006). pH-dependent iron oxide precipitation in a subterranean estuary. *Journal of Geochemical Exploration*, *88*, 399–403. https://doi.org/10.1016/j.gexplo.2005.08.084

Spiteri, C., Slomp, C. P., Regnier, P., Meile, C., & Van Cappellen, P. (2007). Modelling the geochemical fate and transport of wastewater-derived phosphorus in contrasting groundwater systems. *Journal of Contaminant Hydrology*, *92*, 87–108. https://doi.org/10.1016/j.jconhyd.2007.01.002

Spiteri, C., Slomp, C. P., Charette, M. A., Tuncay, K., & Meile, C. (2008). Flow and nutrient dynamics in a subterranean estuary (Waquoit Bay, MA, USA): Field data and reactive transport modeling. *Geochimica et Cosmochimica Acta*, *72*, 3398–3412. https://doi.org/10.1016/j.gca.2008.04.027

Sugimoto, R., Honda, H., Kobayashi, S., Takao, Y., Tahara, D., Tominaga, O., & Taniguchi, M. (2015). Seasonal changes in submarine groundwater discharge and associated nutrient transport into a tideless semi-enclosed embayment (Obama Bay, Japan). *Estuaries and Coasts*, *39*(1), 13–26. https://doi.org/10.1007/s12237-015-9986-7

Swarzenski, P. W., Simonds, F. W., Paulson, A. J., Kruse, S., & Reich, C. (2007). Geochemical and geophysical examination of submarine groundwater discharge and associated nutrient loading estimates into Lynch Cove, Hood Canal, WA. *Environmental Science & Technology*, *41*, 7022–7029. https://doi.org/10.1021/es070881a

Talbot, J. M., Kroeger, K. D., Rago, A., Allen, M. C., & Charette, M. A. (2003). Nitrogen flux and speciation through the subterranean estuary of Waquoit Bay, Massachusetts. *Biological Bulletin*, *205*(2), 244–245. https://doi.org/10.2307/1543276

Teixeira, C., Magalhães, C., Joye, S. B., & Bordalo, A. A. (2013). The role of salinity in shaping dissolved inorganic nitrogen and N_2O dynamics in estuarine sediment–water interface. *Marine Pollution Bulletin*, *66*(1-2), 225–229. https://doi.org/10.1016/j.marpolbul.2012.11.004

Teixeira, C., Magalhães, C., Joye, S. B., & Bordalo, A. A. (2014). The contribution of anaerobic ammonium oxidation to nitrogen loss in two temperate eutrophic estuaries. *Estuarine, Coastal and Shelf Science*, *143*, 41–47. https://doi.org/10.1016/j.ecss.2014.03.023

Teixeira, C., Magalhães, C., Joye, S. B., & Bordalo, A. A. (2016). Response of anaerobic ammonium oxidation to inorganic nitrogen fluctuations in temperate estuarine sediments. *Journal of Geophysical Research: Biogeosciences*, *121*, 1829–1839. https://doi.org/10.1002/2015JG003287

Trimmer, M., Nicholls, J. C., & Deflandre, B. (2003). Anaerobic ammonium oxidation measured in sediments along the Thames estuary, United Kingdom. *Applied and Environmental Microbiology*, *69*(11), 6447–6454. https://doi.org/10.1128/AEM.69.11.6447-6454.2003

Tse, K. C., & Jiao, J. J. (2008). Estimation of submarine groundwater discharge in Plover Cove, Tolo Harbour, Hong Kong by ^{222}Rn. *Marine Chemistry*, *111*, 160–170. https://doi.org/10.1016/j.marchem.2008.04.012

Tuominen, L., Heinänen, A., Kuparinen, J., & Nielsen, L. P. (1998). Spatial and temporal variability of denitrification in the sediments of the northern Baltic proper. *Marine Ecology Progress Series*, *172*, 13–24. https://doi.org/10.3354/meps172013

Xu, F. L., Lam, K. C., Zhao, Z. Y., Zhan, W., Chen, Y. D., & Tao, S. (2004). Marine coastal ecosystem health assessment: A case study of the Tolo Harbour, Hong Kong, China. *Ecological Modelling*, *173*, 355–370. https://doi.org/10.1016/j.ecolmodel.2003.07.010

Yang, J.-S., Choi, H.-Y., Jeong, H.-J., Jeong, J.-Y., & Park, J.-K. (2000). The outbreak of red tides in the coastal waters off Kohung, Chonnam, Korea: 1. Physical and chemical characteristics in 1997. *The Sea*, *5*(1), 16–26.